ADVANCED OPTICAL MATERIALS
www.advopticalmat.de

Check for updates

Wavelength-Linearly-Dependent and Polarization-Sensitive Perfect Absorbers based on Optically Anisotropic Germanium Selenide (GeSe)

Zhengfeng Guo, Honggang Gu, Yali Yu, Qihang Zhang, Zhongming Wei,* and Shiyuan Liu**

Perfect absorbers, widely utilized in solar energy-harvesting devices, optical communications, sensors, displays, and filters, achieve 100% light absorption. However, perfect absorbers employing micro/nanostructures encounter challenges such as high cost and complexity in simulation and fabrication. Here, novel wavelength-linearly-dependent and polarization-sensitive perfect absorbers utilizing optically anisotropic germanium selenide (GeSe) are proposed. A simple and cost-effective GeSe-SiO_2-Si multilayered optical thin film is constructed and optimized to achieve destructive interference, leading to perfect absorption. The operating wavelength can be linearly tuned from 900 nm to 1300 nm by adjusting the GeSe thickness from 125 nm to 200 nm. Leveraging the significant optical anisotropy, the polarization angle is introduced as an additional parameter to dynamically and finely control the operating wavelength, enabling the creation of polarization-sensitive perfect absorbers. Experimental results validate the feasibility of fabricating and dynamically modulating the proposed wavelength-linearly-dependent and polarization-sensitive perfect absorbers. This study introduces a novel approach for designing and fabricating reconfigurable perfect absorbers utilizing low-symmetry materials, facilitating mass production and on-chip integrated systems.

1. Introduction

Widely applied in solar energy-harvesting devices,[1] optical interconnections and communications,[2] displays and filters,[3] and sensors,[4] perfect absorbers are capable of realizing 100% light absorption.[5] In general, there are two main strategies for designing and producing perfect absorbers. One is based on micro/nanostructures, such as metamaterials or metasurfaces, to achieve perfect absorption.[6] However, these elaborate structures complicate the design and fabrication processes and are expensive. Another type of perfect absorber is made of an optical thin film and can also absorb 100% of electromagnetic waves, benefiting from the destructive interference effect.[3b,7] The operating wavelength can be easily modulated by the layer thickness, and such simple-structure-perfect absorbers are relatively inexpensive compared to those based on micro/nanostructures.

Regardless of the type of perfect absorber mentioned above, their absorption

Z. Guo, H. Gu, Q. Zhang, S. Liu
State Key Laboratory of Intelligent Manufacturing Equipment and Technology
School of Mechanical Science and Engineering
Huazhong University of Science and Technology (HUST)
Wuhan, Hubei 430074, China
E-mail: hongganggu@hust.edu.cn; shyliu@hust.edu.cn

Z. Guo
Innovation Institute
Huazhong University of Science and Technology
Wuhan, Hubei 430074, China

H. Gu
Guangdong HUST Industrial Technology Research Institute
Guangdong Provincial Key Laboratory of Manufacturing Equipment Digitization
Dongguan, Guangdong 523003, China

H. Gu, S. Liu
Optics Valley Laboratory
Wuhan, Hubei 430074, China

Y. Yu, Z. Wei
State Key Laboratory of Superlattices and Microstructures
Institute of Semiconductors
Chinese Academy of Sciences
Beijing 100083, China
E-mail: zmwei@semi.ac.cn

S. Liu
School of Optical and Electronic Information
Huazhong University of Science and Technology
Wuhan, Hubei 430074, China

The ORCID identification number(s) for the author(s) of this article can be found under https://doi.org/10.1002/adom.202303138

DOI: 10.1002/adom.202303138

 © 2024 Wiley-VCH GmbH

features, such as the operating wavelength, may not be changed once their structures have been determined. Hence, there remains a research challenge and trend to reversibly and dynamically modulate the performance of perfect absorbers.[8] By introducing polarization, perfect absorbers become tunable and reconfigurable. However, most reported polarization-sensitive perfect absorbers are designed or fabricated using symmetry-broken micro/nanostructures, such as symmetry-broken metamaterials [9] and metasurfaces,[10] and optical gratings,[11] which increases the cost and complexity of simulation and fabrication. Therefore, further in-depth research efforts are required to design low-cost and simple-structure polarization-sensitive perfect absorbers.

Apart from the superior environmental stability, no toxicity, and rich abundance of composed elements,[12] germanium selenide (GeSe) possesses an appropriate bandgap (≈1.2 eV [13]) and high level of light absorption coefficient (≈10^5 cm^{-1} [14]) in the visible region, making it an outstanding candidate for optical and optoelectronic devices, such as solar cells [15] and photodetectors.[12,16] More excitingly, GeSe exhibits giant and attractive optical anisotropy due to its low-symmetry puckered lattice structure with the space group $D_{2h}^{16}-Pcnm$ (No. 62),[17] which is even lower than the similar pucker-like structure of black phosphorus (BP) with its space group of $D_{2h}^{18}-Cmca$ (No. 64).[18] The optical anisotropy not only brings much richer physics, such as birefringence [19] and dichroism,[20] but also offers an extra degree of freedom to tune the optical properties to achieve polarization-sensitive applications. Recently, most research has focused on the qualitative identification and observation of the optically anisotropic phenomena of GeSe with the help of polarization absorption [12] or reflection [21] spectroscopy and polarization-resolved optical microscopy.[22] However, there is still a need for a quantitative evaluation index of optical anisotropy that will help to rationally design polarization-sensitive optical devices and systems and provide a comprehensive performance prediction. At present, a significant portion of the research on quantitatively investigating the optical anisotropy of GeSe has focused on theoretically predicting its complex refractive indices.[22–23] Another main part of research attention has been paid to experimentally measuring [14,21] its absorption coefficient spectra which is only related to the extinction coefficient k. Therefore, there is a lack of reliable and complete GeSe's complex refractive index tensor to quantitatively and comprehensively investigate the optical anisotropy and rationally design optical devices like perfect absorbers.

In this study, we designed and fabricated wavelength-linearly-dependent and polarization-sensitive perfect absorbers based on simple structures and low-cost optical thin films by modulating the layer thicknesses of GeSe and incident polarization angles. After qualitatively observing and identifying the optical anisotropic characteristics of GeSe for the first time using azimuth-dependent off-diagonal Mueller matrix spectra and polarization-sensitive reflection spectra, Mueller matrix spectroscopic ellipsometry was utilized to acquire the reliable and complete complex refractive index tensor and the derived birefringence and dichroism to quantitatively evaluate the optical anisotropy of GeSe. Based on these results, the GeSe-SiO_2-Si multilayered optical thin film was constructed, and the layer thickness of GeSe was optimized to achieve destructive interference and ultimately perfect light absorption. Considering GeSe's giant optical anisotropy, we further introduced the polarization angles as an additional degree of freedom to dynamically and finely modulate the operating wavelength, obtaining tunable and reconfigurable perfect absorbers. Finally, we experimentally confirmed the modulation rules of both the GeSe layer thickness and the polarization angle on the proposed GeSe-based perfect absorbers.

2. Results and Discussion

2.1. Optical Anisotropy of GeSe

Figure 1a demonstrates the low-symmetry lattice structure of layered GeSe, belonging to the orthorhombic system. Similar to BP,[18] GeSe exhibits a pucker-like structure in the plane, where Ge and Se atoms alternately and covalently array along the b and c-axes to respectively form the zigzag (ZZ) and armchair (AC) structures.[12,17] Along the a-axis, however, the interlayer interaction is the van der Waals (vdW) force instead of a covalent interaction in the b-c plane due to its layered nature.[22] Thus, GeSe can be easily exfoliated into few-layered nanosheets, as shown in Figure S1 (Supporting Information). The thickness of the GeSe nanosheet shown in Figure S1 (Supporting Information) was ≈40 nm, as measured by atomic force microscopy (AFM). The low-symmetry structure of GeSe is confirmed by the Raman spectrum in Figure 1b, with three Raman vibration modes, namely A_g^1, B_{3g}, and A_g^3, are respectively identified at the peak Raman shifts of 79, 148, and 186 cm^{-1}, consistent with previously reported results.[24] Additionally, the inset schematic diagrams in Figure 1b illustrate the lattice vibrations corresponding to the mentioned Raman modes of GeSe. Specifically, the A_g^1 mode represents the vibration where two sublayers move opposite to each other, while the B_{3g} and A_g^3 modes are respectively twisting and stretching vibrations in the b-c plane.[24a,25]

The pucker-like low-symmetry structure brings giant optical anisotropy, which can be identified by azimuth-dependent off-diagonal Mueller matrix spectra. The values of the off-diagonal Mueller matrix elements depend not only on the magnitude of optical anisotropy but also on the orientation of GeSe's in-plane crystal axes (i.e., b- or c-axis).[26] Here, we take the spectra of M_{41}, the off-diagonal Mueller matrix element in the fourth row and first column, as an example shown in Figure 1c. The absolute value of M_{41} was as high as 0.3, indicating the giant optical anisotropy of GeSe at the peak wavelength of 420 nm. Moreover, the M_{41} value varies with the alteration of azimuth from 0 to 180°, achieved by rotating the GeSe sample in its b-c plane, as shown in Figure S2 (Supporting Information). To clarify the relationship between the M_{41} value and the orientation of GeSe's in-plane crystal axes, Figure 1d illustrates M_{41} versus the azimuth at a peak wavelength of 420 nm. When the optical axis of GeSe was parallel or perpendicular to the incident plane, as shown in Figure S2 (Supporting Information), M_{41} turned to zero.[26] In Figure 1d, M_{41} is zero at approximately azimuth angles of 45 and 135°, indicating that the optical axis of GeSe is parallel or perpendicular to the incident plane at those azimuths.

The giant optical anisotropy of GeSe has also been observed in the polarization-sensitive reflection spectra, as shown in Figure 1e,f. Figure 1e demonstrates that the ratio of maximum to minimum reflectance is up to 2, indicating GeSe's giant

© 2024 Wiley-VCH GmbH

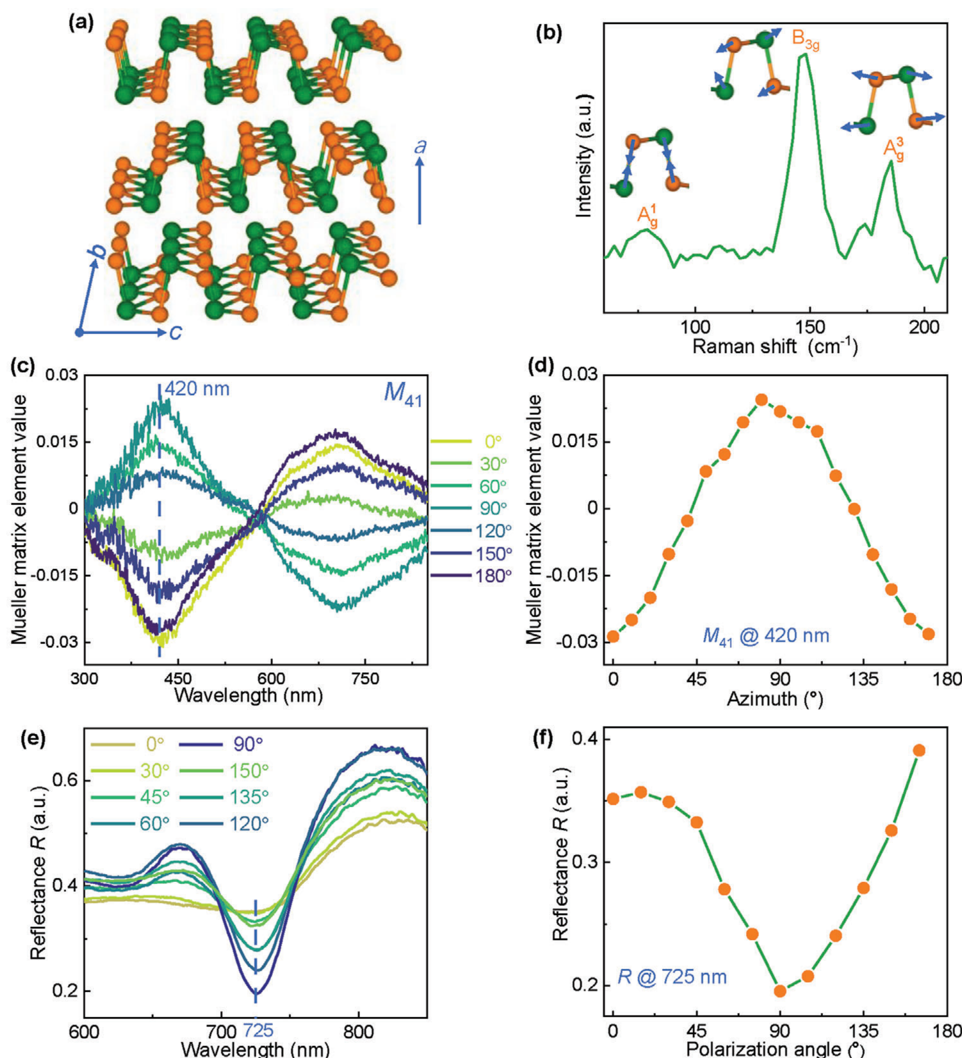

Figure 1. Low-symmetry lattice structure and optical anisotropy of GeSe. a) Low-symmetry lattice structure of GeSe. b) Raman spectrum with an inserted schematic diagram of lattice vibration for different Raman modes. c) Azimuth-dependent Mueller matrix element M_{41} spectra. d) M_{41} element value at the peak wavelength of 420 nm varied with the azimuth. e) Polarization-sensitive reflection spectra. f) Reflectance at the wavelength of 725 nm versus polarization angle.

optical anisotropy. Furthermore, the reflectance spectra of GeSe alter with the increasing polarization angle, and the curve of reflectance versus polarization angle at the wavelength of 725 nm is illustrated in Figure 1f to figure out their relation. The reflectance of GeSe first decreases and then increases with the increasing polarization angle, indicating GeSe's polarization sensitivity.

To quantitatively evaluate the optical anisotropy of GeSe, Mueller matrix spectroscopic ellipsometry was utilized to acquire its complete dielectric tensor, as shown in **Figure 2a**, and the complex refractive index tensor (which can be converted from the dielectric tensor) is shown in Figure 2b. More details about the process of ellipsometric data acquisition as well as the conversion of the dielectric tensor can be found in Supporting Notes S1 and S2 (Supporting Information), respectively. Because GeSe's low-symmetry structure belongs to the orthorhombic crystal system, the complex refractive index tensor is diagonal, and its elements, namely, the complex refractive indices, are along GeSe's crystal axes, i.e., N_a, N_b, and N_c. In Figure 2b, we denote N_b and N_c as N_{ZZ} and N_{AC} respectively. In addition, the refractive index n and the extinction coefficient k constitute the complex refractive index N (= $n + ik$). As mentioned above, the vdW interaction occurs along the a-axis and obviously differs from the covalent interactions along the AC and ZZ directions. Therefore, a Cauchy model was adopted to describe the complex refractive index along the a-axis [27] whereas Tauc-Lorentz oscillators were used to describe those along the AC and ZZ directions [28] (See Note S1, Supporting Information for more details). As shown in Figure 2b, N_a exhibited entirely different curve shapes than N_{ZZ} and N_{AC}. In addition to this out-of-plane optical anisotropy, the in-plane optical anisotropy of GeSe is demonstrated by the discrepancies of N_{ZZ} and N_{AC} in the peak positions and intensities, which may originate from the puckered low-symmetry structure in the b-c plane.[26a,b] In brief, N_a, N_{ZZ}, and N_{AC} in Figure 2b display many differences in peak positions and intensities and even

© 2024 Wiley-VCH GmbH

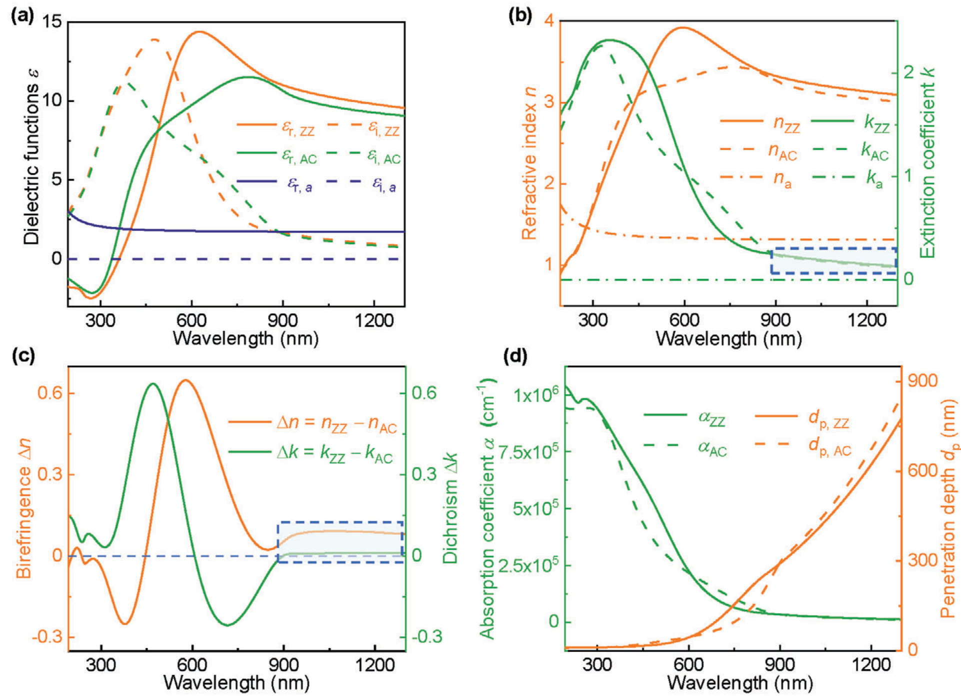

Figure 2. Quantitative characterization of the optically anisotropic GeSe. a) dielectric tensor, b) complex refractive index tensor, c) birefringence Δn and dichroism Δk, and d) absorption coefficient α and penetration depth d_p.

curve shapes, demonstrating the giant optical anisotropy of GeSe in a quantitative view.

The birefringence Δn ($= n_{ZZ} - n_{AC}$) and dichroism Δk ($= k_{ZZ} - k_{AC}$) were calculated as quantitative indices to evaluate the optical anisotropy of GeSe, as shown in Figure 2c. The huge value of the Δn and the Δk indicate GeSe's giant optical anisotropy once again, whose maximum is 0.65 (for Δn_{max}) and 0.64 (for Δk_{max}), respectively. The measured Δn and Δk in this study share the same trend as the reported theoretical results [22] and Δn_{max} is superior to those of many other low-symmetry materials such as BP ($\Delta n_{BP} = 0.15$),[29] ReS_2 ($\Delta n_{ReS2} = 0.06$),[30] $ZrTe_5$ ($\Delta n_{ZrTe5} = 0.58$),[26a] and tellurene ($\Delta n_{tellurene} = 0.48$).[26b]

Additionally, we observed weak absorption features over the wavelength range above ≈900 nm (the marked area in Figure 2b), where k_{ZZ} and k_{AC} gradually decreased to zero. Such weak absorption features are also reflected in the absorption coefficient α and the penetration depth d_p of the *b*-*c* plane, as shown in Figure 2d. Here, the absorption coefficients along the AC or ZZ directions, i.e., α_{AC} or α_{ZZ} respectively, are defined as [26c]

$$\alpha_i = \frac{4\pi k_i}{\lambda}, i = \text{ACorZZ} \quad (1)$$

where λ denotes the wavelength (cm). The penetration depth along the AC or ZZ direction $d_{p,\ i}$ (i = AC or ZZ) is the reciprocal of α_i [26c].

$$d_{p,i} = \frac{1}{\alpha_i}, i = \text{ACorZZ}. \quad (2)$$

Both α_{AC} and α_{ZZ} are at high levels of about 10^5 cm^{-1} in the visible light region, which is consistent with previous report.[14] However, in the near-infrared region (≈900–1300 nm in this study), α_{AC} and α_{ZZ} drop sharply to zero, and such weak absorption features can also be visually observed by $d_{p,\ AC,}$ and $d_{p,\ ZZ}$, owing to their rapid rise within the same wavelength region in Figure 2d.

2.2. Design Thoughts of Perfect Absorbers Based on Optically Anisotropic GeSe

In general, the weak absorption of materials causes destructive interference in the corresponding layer structure,[31] which is the key to designing perfect absorbers. Furthermore, optical anisotropy separates the occurring wavelengths for the destructive interference of p- and s-light due to the birefringence Δn [32], making perfect absorbers reversibly and dynamically tunable. Here, p-light and s-light are defined based on the different oscillatory directions of their electric fields, which are also known as p- and s-polarized light. The electric field of p-light oscillates within the plane of incidence, while the oscillatory direction of s-light's electric field is vertical to the plane of incidence.[26c] In the marked near-infrared region (> ≈900 nm) of Figure 2c, Δn of GeSe is maintained at about 0.1, which may lead to the separation of the destructive interference wavelength for p- and s-light. Moreover, the Δk of GeSe is nearly zero in this near-infrared region, suggesting that p- and s-light may have the same intensity at the destructive interference wavelength.

Based on the above discussion, we have adopted the GeSe-SiO_2-Si multilayered optical thin-film structure, i.e., optically anisotropic GeSe on a silicon (Si) substrate with a SiO_2 oxide layer, to achieve perfect absorption, as shown in **Figure 3a**.

 © 2024 Wiley-VCH GmbH

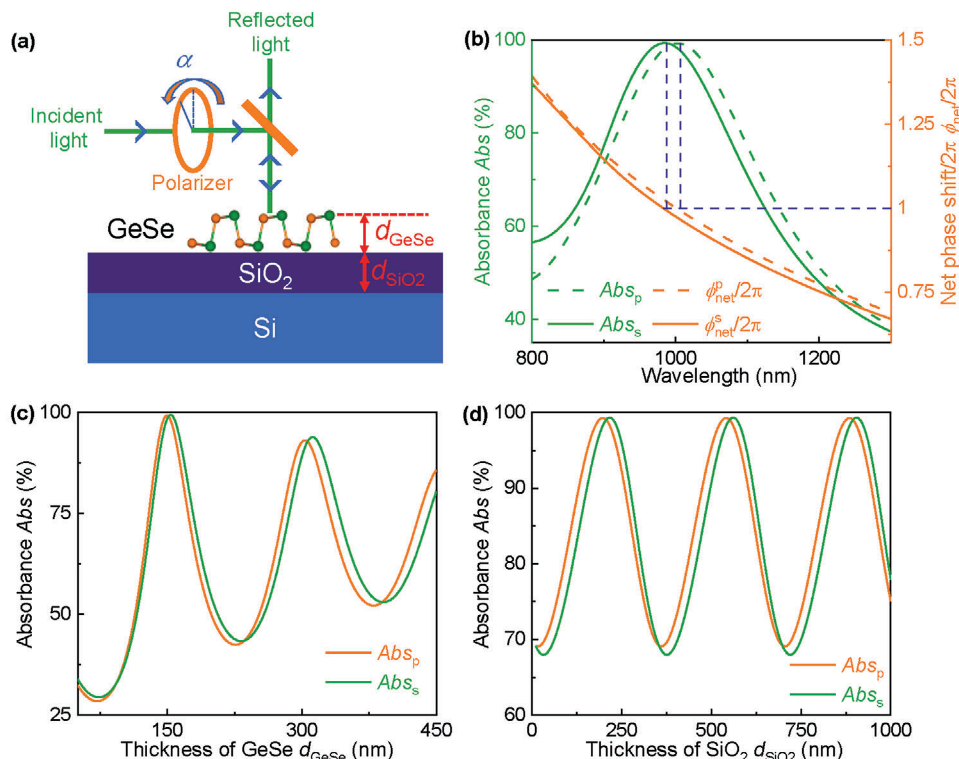

Figure 3. Design thoughts of perfect absorbers based on optically anisotropic GeSe. a) Schematic diagram of the perfect absorber based on an optical thin film structure tuned by the incident polarization angle, where α is the polarization angle. b) Absorbance of s- and p-light (Abs_s and Abs_p) and the net phase shift (ϕ^s_{net} and ϕ^p_{net}) of the optical thin film with the thicknesses of GeSe layer and SiO_2 layer (d_{GeSe} and d_{SiO_2}) set at 150 and 200 nm, respectively. Abs_s and Abs_p varied with c) d_{GeSe} and d) d_{SiO_2} at the wavelength of 1000 nm, where d_{GeSe} and d_{SiO_2} are respectively set at 150 and 200 nm.

Additionally, the incident polarization angle can be reversibly and dynamically tuned using a linear polarizer. As a lossless dielectric material, the SiO_2 layer adds an extra degree of freedom to regulate the destructive interference effect by altering its thickness (d_{SiO_2}) in addition to that of GeSe (d_{GeSe}).[33] Furthermore, the Si substrate was selected because it is compatible with integrated optoelectronics and on-chip systems.[32a] Since the Si substrate may not allow the transmission of incident light ($T = 0$), the absorbance of s- or p-light (Abs_s or Abs_p) is accordingly calculated by the corresponding reflectance R_j (j = s or p).

$$Abs_j = 1 - R_j, j = \text{s or p}. \quad (3)$$

In Equation 3, the reflectances of s- and p-light, R_s and R_p, are acquired from the transfer matrix method [32a,34], where the complex refractive indices along the AC and ZZ directions are taken as the input parameters to independently calculate Abs_s and Abs_p, respectively. For convenience, the vibrational directions of the s- and p-light beams remain parallel to the AC and ZZ directions of GeSe, respectively, at normal incidence all the time. Since the adopted thicknesses of GeSe (≥ 100 nm) in the calculations are much thicker than those of few-layer 2D GeSe (approximately several nanometers), the quantum confinement effect [35] does not play the leading role, and the refractive indices n and the extinction coefficients k of the 2D GeSe film are probably almost the same as those of bulk GeSe. Therefore, in our theoretical calculations, the refractive indices n and the extinction coefficients k of the 2D GeSe film are adapted from those of the single-crystal sample shown in Figure 2b.

For the multilayered optical thin-film structure, one of the conditions for the destructive interference to realize perfect absorption is the net phase shift ϕ_{net} of integer multiples of 2π.[7b] Further details are provided in Supporting Note S3 (Supporting Information). As illustrated in Figure 3b, the wavelengths corresponding to the net phase shift ϕ_{net} of 2π for both s- and p-light are equal to those of $Abs_{s,\,max}$ and $Abs_{p,\,max}$, i.e. operating wavelength λ_{ope}. Therefore, it is of great importance to optimize the suitable layer thicknesses, i.e., d_{GeSe} and d_{SiO_2}, to achieve a net phase shift ϕ_{net} of 2π (or its integer multiple) and ultimately perfect absorption. As shown in Figure 3c,d, we have further theoretically calculated the absorbance varied with d_{GeSe} and d_{SiO_2}. In Figure 3c, the maximum absorbance of the GeSe-SiO_2-Si multilayered optical thin film for both s- and p-light decreases with d_{GeSe} increasing due to the stronger absorption for the thicker GeSe layer. However, in Figure 3d, the maximum absorbance remains unchanged despite the increase in d_{SiO_2}, owing to the SiO_2's characteristic of being a lossless dielectric. Due to the optical anisotropy of GeSe, the s- and p-light's absorbance coefficients, Abs_s and Abs_p are separated from each other during the variation of d_{GeSe} and d_{SiO_2}, offering an extra degree of freedom to reversibly and dynamically tune the operating wavelength λ_{ope} of the perfect absorbers.

© 2024 Wiley-VCH GmbH

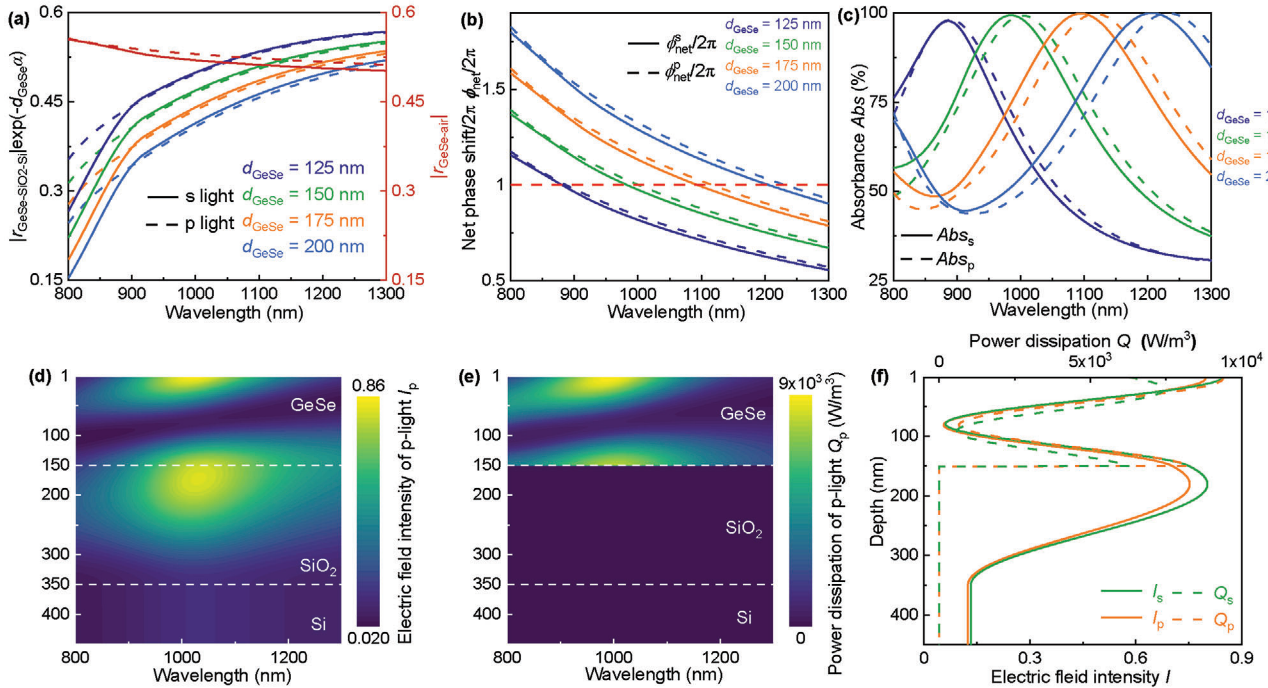

Figure 4. Wavelength-linearly-dependent perfect absorber modulated by layer thicknesses. a) Amplitude condition of perfect absorption, b) net phase shift/2π $\phi_{net}/2\pi$, and c) absorbance *Abs* spectra for both s- and p-light varied with the thickness of GeSe d_{GeSe} of 125, 150, 175, and 200 nm. Distribution of p-light's d) electric field intensity I_p spectra and e) power dissipation Q_p spectra of GeSe (150 nm)-SiO_2-Si multilayered film. f) Distribution of electric field intensity *I* spectra and power dissipation *Q* spectra for both s and p-light at their operating wavelength.

2.3. Wavelength-Linearly-Dependent Perfect Absorber Modulated by Layer Thicknesses

As shown in Figure S3a (Supporting Information), the net phase shift of s-(p-)light $\phi_{net}^{s(p)}$ approaches (but does not equal) 2π at the wavelength of 800 nm when d_{GeSe} is 100 nm, leading to nearly perfect absorption at such wavelengths (Figure S3b, Supporting Information). Moreover, thicker d_{GeSe} layers (250, 350, and 450 nm) result in net phase shifts of 4, 6, and 8π, as depicted in Figure S3a (Supporting Information). Although Abs_s (Abs_p) of the optical thin film with these thicker d_{GeSe} layers reaches its maximum at the corresponding wavelengths of $\phi_{net}^{s(p)}$ 4, 6, and 8π in Figure S3b (Supporting Information), there remains significant room for optimizing Abs_s or Abs_p to reach unity (100%).

To achieve perfect absorption, amplitude and phase conditions must be satisfied simultaneously.[7b] The amplitude condition is[7b]

$$\left|r_{GeSe-air}^{s(p)}\right| = \left|r_{GeSe-SiO_2-Si}^{s(p)}\right| \exp\left(-\frac{4\pi d_{GeSe} k_{AC(ZZ)}}{\lambda}\right) = \left|r_{GeSe-SiO_2-Si}^{s(p)}\right| \exp\left(-d_{GeSe}\alpha_{AC(ZZ)}\right), \quad (4)$$

where $r_{air-GeSe}^{s(p)}$ and $r_{GeSe-SiO_2-Si}^{s(p)}$ are the amplitude reflection coefficients of s-(p-)light for the air-GeSe structure and GeSe-SiO_2-Si structure, respectively. Further details are provided in Supporting Note S3 (Supporting Information). As shown in Figure S3a (Supporting Information), the amplitude condition of perfect absorption was calculated for both s- and p-light, which varied with d_{GeSe}. The phase condition is the net phase-shift $\phi_{net}^{s(p)}$ of integer multiples of 2π.

For relatively thinner thicknesses of GeSe (such as 100 nm), although the amplitude condition is satisfied as shown in Figure S3a (Supporting Information), the net phase shift $\phi_{net}^{s(p)}$ does not meet the condition of being an integer multiple of 2π, as illustrated in Figure S3b (Supporting Information). Consequently, perfect absorption cannot be achieved when the GeSe thickness is relatively low. However, if the GeSe thickness is much greater (e.g., 250, 350, and 450 nm), the amplitude condition cannot be reached despite satisfying the phase condition. Since the left side of Equation 4, i. e., $r_{air-GeSe}^{s(p)}$, is independent of the thickness of GeSe, and the right side of Equation 4 varies with the thickness of GeSe, there exists a certain thickness range of GeSe to satisfy the amplitude condition accordingly.

We further refined the d_{GeSe} to values such as 125, 150, 175, and 200 nm to achieve both the amplitude and phase conditions simultaneously, as illustrated in **Figure** 4a,b. By combining Figure 4b,c, one can find that perfect absorption occurs at the wavelength corresponding to the net phase shift ϕ_{net} of 2π. The maximum absorbance values of s- and p-light, $Abs_{s,\,max,}$ and $Abs_{p,\,max}$, at d_{GeSe} values of 125, 150, 175, and 200 nm are also listed in **Table** 1. All $Abs_{s,\,max}$ and $Abs_{p,\,max}$ values are above 97% and even ≈99%, indicating perfect absorption at these GeSe thicknesses. Moreover, the operating wavelength λ_{ope} of the perfect absorber, corresponding to $Abs_{s,\,max}$ or $Abs_{p,\,max}$, is red-shifted with increasing d_{GeSe} (Table 1). Furthermore, s- and p-light can be used to further finely tune λ_{ope} (Figure 4c and Table 1). Therefore, λ_{ope} can be reversibly and dynamically regulated simply by

 © 2024 Wiley-VCH GmbH

Table 1. Maximum absorbance of s- and p-light $Abs_{s,\,max}$ and $Abs_{p,\,max}$ and their corresponding wavelengths, also the wavelengths of net phase shift of 2π, at the d_{GeSe} of 125, 150, 175, and 200 nm.

d_{GeSe} [nm]	$Abs_{s,\,max}$ [%]	$Abs_{s,\,max}$ wavelength [nm]	$Abs_{p,\,max}$ [%]	$Abs_{p,\,max}$ wavelength [nm]
125	97.74	886	98.08	890
150	99.36	985	99.29	1003
175	99.85	1095	99.78	1118
200	99.99	1206	99.95	1232

altering s- and p-light, allowing for the acquisition of reconfigurable perfect absorbers.

Throughout the entire process of the theoretical calculations mentioned above, the d_{SiO_2} thickness was fixed at 200 nm. The contour maps of Abs_s and Abs_p spectra varied with d_{SiO_2} are respectively illustrated in Figure S4 and Table S2 (Supporting Information) to explain the rationale for selecting this d_{SiO_2}. Additionally, we investigated the influence of the Si thickness on perfect absorption, as demonstrated in Figure S5 (Supporting Information). Further details can be found in Supporting Notes S4 and S5 (Supporting Information).

To explore the absorption mechanism, we calculated the distribution of electric field intensity I spectra and power dissipation Q [34] spectra of the optical thin film. As shown in Figure 4d and Figure S6a–c (Supporting Information), the maximum electric field intensities of p-light, $I_{p,max}$, for d_{GeSe} values of 150 nm, as well as 125, 175, and 200 nm, are mainly distributed at the air-GeSe and GeSe-SiO_2 interfaces. The $I_{p,\,max}$ wavelength was identified with the operating wavelength, suggesting that destructive interference likely causes $I_{p,\,max}$. Q represents the power dissipated during the propagation process of the electromagnetic field, which can also be regarded as the absorbed power in each layer.[34] Different from the distribution of I_p spectra, the power dissipation of p-light, Q_p, for different d_{GeSe} values in Figure 4f and Figure S6d–f (Supporting Information) is primarily distributed at the upper and lower interfaces in the GeSe layer, with no distribution in the SiO_2 layer due to its lossless dielectric properties. The electric field intensity I_s spectra and power dissipation Q_s spectra of s-light share almost identical distribution characteristics, as depicted in Figure S7 (Supporting Information). The wavelength corresponding to the maximum power dissipation is also consistent with the operating wavelength for different thicknesses of the GeSe layer. Therefore, absorption at the upper and lower interfaces of the GeSe layer results in perfect absorption. The main differences between I_p (Q_p) and I_s (Q_s) are their wavelengths at the I_{max} (Q_{max}) and I_{max} (Q_{max}) intensities shown in Figures S8 (Supporting Information) and Figure 4f respectively, which are attributed to the giant optical anisotropy of GeSe.

The influence of variations in d_{GeSe} is also discussed. Besides the redshift of $I_{s(p),\,max}$ wavelength, the electric field intensity $I_{s(p),\,max}$ for both p- and s-light increases with the increase in d_{GeSe}, respectively, as shown in Figure 4d, and Figures S6a–c, and S7a–d (Supporting Information). However, as illustrated in Figure 4e, Figures S6d–f, and S7e–h (Supporting Information), the maximum s-(p-)light power dissipation $Q_{s(p),\,max}$ does not seem to share a similar variation trend with $I_{s(p),\,max}$ when d_{GeSe} becomes thicker. $Q_{s(p)}$ in the GeSe layer is calculated as follows:[34]

$$Q_{s(p)} = \pi c \epsilon_0 \frac{n_{AC(ZZ)} k_{AC(ZZ)}}{\lambda} I_{s(p)}, \tag{5}$$

where c and ϵ_0 are the speed of light and permittivity in vacuum, respectively. Equation 5 indicates that the complex refractive indices of GeSe ($n_{AC(ZZ)}$ and $k_{AC(ZZ)}$) have a considerable impact on $Q_{s(p)}$ in the GeSe layer. As the redshift of the $Q_{s(p),\,max}$ wavelength and the decline of both $n_{AC(ZZ)}$ and $k_{AC(ZZ)}$ within the concerned wavelength range (≈900 to 1300 nm) in Figure 1b, $Q_{s(p),\,max}$ no longer varies only with $I_{s(p),\,max}$, and the complex refractive indices of GeSe has a greater influence on it. Therefore, the power dissipation $Q_{s(p)}$ related to $d_{GeSe} = 125$ nm has the highest value at the operating wavelength λ_{ope} among those $Q_{s(p)}$ related to thicker GeSe layers. However, its absorption $Abs_{s(p)}$ was still the lowest compared with other $Abs_{s(p)}$ values related to thicker GeSe layers, as shown in Table 1. The relationship between $Abs_{s(p)}$ and the power dissipation $Q_{s(p)}$ is as follows:

$$Abs_{s(p)} = \frac{\int Q_{s(p)}(z)dz}{S_0^{s(p)}}, \tag{6}$$

As z stands for the layer thickness of GeSe-SiO_2-Si multilayered optical thin film, Equation 6 indicates that $Abs_{s(p)}$ not only correlates with $Q_{s(p)}$ but also depends on the d_{GeSe}. According to Table 1, as d_{GeSe} increases, $Abs_{s(p)}$ also increases, highlighting the significant role of d_{GeSe} in determining $Abs_{s(p)}$.

2.4. Polarization-Sensitive Reconfigurable Perfect Absorbers

Based on the geometrical relationship between the incident reflected electric field and its components along the AC and ZZ directions illustrated in Figure S9 (Supporting Information), the absorbance Abs varies with the polarization angle α and is obtained as:

$$Abs(\alpha) = 1 - R_s \cos^2\alpha - R_p sin^2\alpha \tag{7}$$

Supporting Note S6 (Supporting Information) provides further details regarding the derivation of $Abs(\alpha)$. Considering the symmetry of GeSe's lattice structure, five representative polarization angles (α = 0, 30, 45, 60, and 90°) were selected to demonstrate the variation in Abs of the GeSe (d_{GeSe} = 160 nm)-SiO_2-Si multilayered optical thin film in **Figure 5**a. The maximum absorbance Abs_{max} value remains nearly constant with these representative polarization angles, while the operating wavelength λ_{ope} varies among them, as shown in Figure 5b, which provides an enlarged view of Figure 5a.

As illustrated in Figure 5c, the operating wavelength λ_{ope} varied with d_{GeSe} and α. The λ_{ope} ranges from ≈900 to 1300 nm and can be modulated almost linearly by d_{GeSe} ranging from ≈125 to 200 nm. Furthermore, λ_{ope} can be finely modulated using a representative α. This fine modulation of λ_{ope} by α is dynamic and reversible, resulting in reconfigurable perfect absorbers.

Here, we elucidate the linear relationship between the operating wavelength λ_{ope} and the thickness of GeSe; further details are

© 2024 Wiley-VCH GmbH

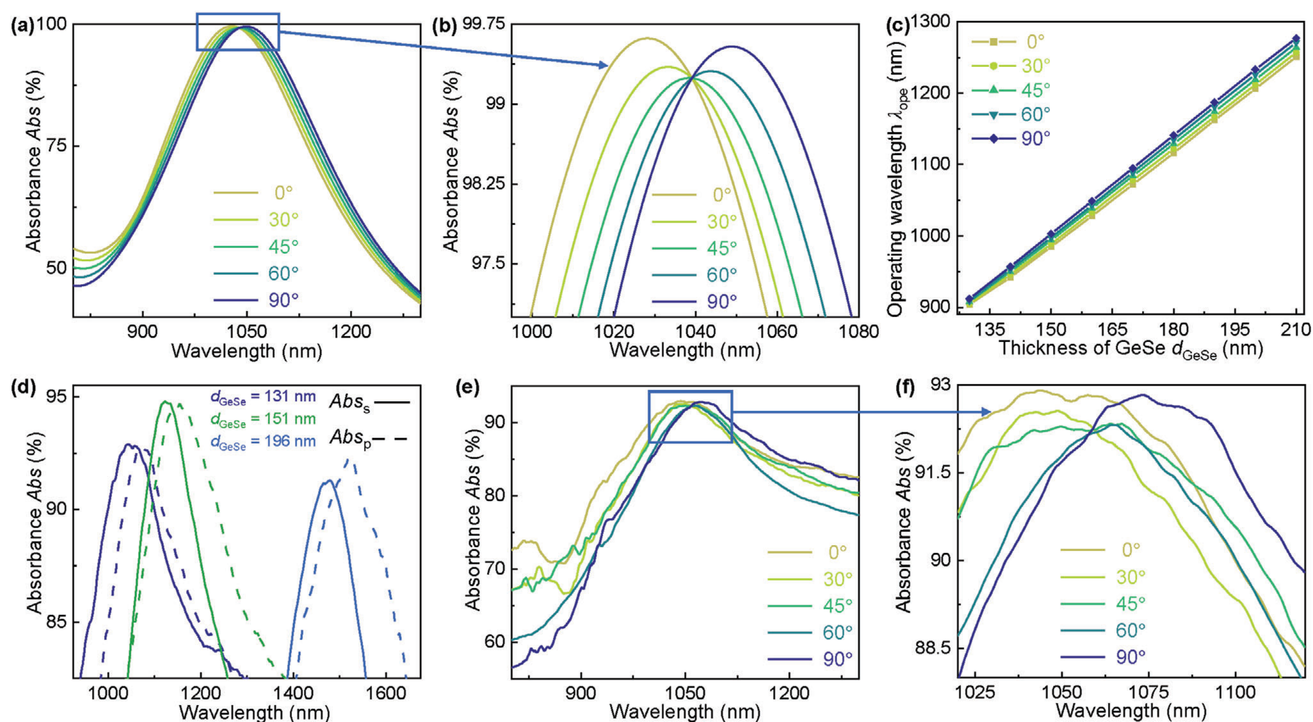

Figure 5. Polarization-sensitive reconfigurable perfect absorbers. a) The absorbance *Abs* varied with the polarization angle α and b) an enlarged view at its peak, corresponding to a thickness of GeSe d_{GeSe} of 160 nm. c) Operating wavelength λ_{ope} varied with d_{GeSe} and α. d) The absorbance Abs_s and Abs_p of exfoliated GeSe nanosheets-based perfect absorbers with different thicknesses of GeSe d_{GeSe}, and e) the *Abs* versus α with f) an enlarged view at the peak, corresponding to d_{GeSe} of 131 nm.

provided in Supporting Note S7 (Supporting Information). As depicted in Figure 3b, the wavelengths corresponding to a net phase shift ϕ_{net} of 2π for both the s- and p-lights are equivalent to the operating wavelength λ_{ope}. Therefore, according to the phase condition of perfect absorption, we can infer the relationship between the operating wavelength λ_{ope} and the thickness of GeSe d_{GeSe} as expressed in Equation S23 (Supporting Information). As illustrated in Figure S10 (Supporting Information), $\phi^{s(p)}_{GeSe-SiO_2-Si}$, the s-(p-)light argument of the corresponding amplitude reflection coefficient for the GeSe-SiO_2-Si structure shares an almost identical decreasing tendency as the refractive index of GeSe $n_{AC(ZZ)}$, thereby establishing a linear relationship between the operating wavelength and GeSe thickness.

The theoretical calculations of perfect absorbers modulated by d_{GeSe} and α were experimentally confirmed. As demonstrated in Figure S11 (Supporting Information), GeSe nanosheets of varying thicknesses were exfoliated on a Si substrate with a SiO_2 oxide layer (d_{SiO_2} = 200 nm). The thicknesses of the GeSe nanosheets, as measured by AFM, fell within the thickness range of GeSe (125–200 nm), consistent with the thickness range of d_{GeSe} in the theoretical calculations. Prior to measuring the *Abs* of the optical thin film, the orientation of the GeSe in-plane crystal axes needed to be determined using polarization-resolved optical microscopy (PROM [22,30]). As an example, we consider the GeSe nanosheet with a thickness of 131 nm. Under the cross-polarized configuration of the PROM (where the polarizer and analyzer in Figure S12a (Supporting Information) are perpendicular to each other), the brightness of the GeSe nanosheet is minimized when the AC or ZZ axes are oriented vertically or parallelly to the polarizer (i.e., 0 or 90° in Figure S12b, Supporting Information).[22,30] Therefore, the in-plane crystal axes orientation of exfoliated GeSe nanosheets with different thicknesses can be determined in this manner.

The *Abs* values based on different thicknesses of the exfoliated GeSe nanosheets are illustrated in Figure 5d. All the *Abs* for both p- and s-light approach 100%, verifying the perfect absorption of the GeSe-based optical thin films. Additionally, the operating wavelength λ_{ope} experiences a redshift with an increase in the exfoliated GeSe nanosheet thickness, consistent with the theoretically calculated operating wavelength *versus* d_{GeSe}. Moreover, the operating wavelengths of the s- and p-lights exhibit an obvious separation, as depicted in Figure 5d, confirming the preliminary fine modulation of the operating wavelength by the polarization angle.

We also measured the *Abs* of a 131 nm thick GeSe nanosheet-based multilayered optical thin film with five representative polarization angles (α = 0, 30, 45, 60, and 90°) to further confirm the fine and reconfigurable modulation by α. As shown in Figure 5e,f, when the polarization angle changes from 0 to 90°, the operating wavelength λ_{ope} undergoes a finer redshift than that modulated by d_{GeSe}. As mentioned previously, the λ_{ope} modulated by α is dynamic and reconfigurable, consistent with the theoretically calculated results for the same d_{GeSe} and d_{SiO_2} in Figure S13 (Supporting Information).

© 2024 Wiley-VCH GmbH

3. Conclusion

In summary, we have developed wavelength-linearly-dependent and polarization-sensitive perfect absorbers based on optically anisotropic GeSe by modulating the layer thickness and incident polarization angle. Utilizing Mueller matrix spectroscopic ellipsometry, we quantitatively evaluated the giant optical anisotropy of GeSe by acquiring and analyzing its dielectric tensor, complex refractive index tensor, and the derived birefringence Δn and dichroism Δk, with maximum values of 0.65 (for Δn_{max}) and 0.64 (for Δk_{max}), respectively. A simple and cost-effective GeSe-SiO_2-Si multilayered optical thin film was constructed, and the thickness of GeSe (d_{GeSe}) was optimized to achieve destructive interference and consequently, perfect absorption, predominantly occurring at the upper and lower interfaces of the GeSe layer. We observed that the operating wavelength (λ_{ope}) ranging from 900 nm to 1300 nm can be almost linearly modulated by varying d_{GeSe} from 125 nm to 200 nm. Leveraging the optical anisotropy of GeSe, we introduced a polarization angle to dynamically and finely modulate the λ_{ope}, enabling the realization of reconfigurable perfect absorbers. Experimental validation confirmed the modulation effects of both d_{GeSe} and the polarization angle on the proposed wavelength-linearly dependent and polarization-sensitive perfect absorbers.

This study presents a novel design and fabrication of reconfigurable perfect absorbers based on novel low-symmetry materials that are likely to be mass-produced. Additionally, perfect absorbers based on 2D GeSe can be integrated into on-chip systems to ensure it can be miniaturized and integrated, thereby meeting the demand for highly integrated levels in the field of integrated optics and optoelectronics. According to our design thoughts and device principles, such novel low-symmetry materials must simultaneously realize destructive interference (and then perfect absorption at their appropriate thickness) and the separation of the operating wavelength of the perfect absorber. Therefore, both weak-absorption low-symmetry materials with giant birefringence Δn (such as the experimentally reported BP,[29] SnSe,[33] and α-MoO_3 [36]) and lossless low-symmetry materials with giant birefringence Δn (also known as high-performance, well-designed birefringent materials [37]) are probably the two appropriate options.

4. Experimental Section

Synthesis and Exfoliation of GeSe Single Crystals: GeSe single crystals were synthesized using the chemical vapor transport (CVT) method [12] and exfoliated into nanosheets on a Si substrate with a SiO2 oxide layer (d_{SiO_2} = 200 nm). Exfoliated GeSe nanosheets of different thicknesses were then selected within a suitable thickness range (125–200 nm). AFM was used to accurately determine the thickness of the GeSe nanoplates, as shown in Figure S10 (Supporting Information).

Net Phase Shift of s-(p-) Light: The net phase shift of s-(p-)light $\phi_{net}^{s(p)}$ involves the propagation phase shift of the GeSe layer ($\phi_{prop}^{s(p)}$) and the reflective phases of the upper and lower interfaces of GeSe ($\phi_{upper}^{s(p)}$ and $\phi_{lower}^{s(p)}$) at normal incidence, calculated by [38]

$$\phi_{net}^{s(p)} = 2\phi_{prop}^{s(p)} + \phi_{lower}^{s(p)} - \phi_{upper}^{s(p)} = 2 \times \frac{2\pi d_{GeSe} n_{AC(ZZ)}}{\lambda} + \phi_{GeSe-SiO_2-Si}^{s(p)} - \phi_{GeSe-air}^{s(p)} \quad (8)$$

In Equation 7, the first term $\phi_{prop}^{s(p)}$ is the propagation phase shift of s-(p-)light in the GeSe layer, and the second term $\phi_{lower}^{s(p)}$ is the reflective phase for s-(p-)light from the GeSe layer to the SiO_2 layer and ultimately to the Si substrate, which can be acquired by calculating the argument of the amplitude reflection coefficient of s-(p-)light $\phi_{GeSe-SiO_2-Si}^{s(p)}$ using the transfer matrix method,[34] i.e.,

$$r_{GeSe-SiO_2-Si}^{s(p)} = \left| r_{GeSe-SiO_2-Si}^{s(p)} \right| \phi_{GeSe-SiO_2-Si}^{s(p)} \quad (9)$$

In Equation 8, $r_{GeSe-SiO_2-Si}^{s(p)}$ is the amplitude reflection coefficient of s-(p-)light for the GeSe-SiO_2-Si multilayer optical thin film, and the third term $\phi_{upper}^{s(p)}$ is the reflective phase of s-(p-)light from the GeSe layer to the air, which is equal to the argument of the amplitude reflection coefficient of s-(p-) light from the GeSe layer to the air $\phi_{GeSe-air}^{s(p)}$, i e.,

$$r_{GeSe-air}^{s(p)} = \left| r_{GeSe-air}^{s(p)} \right| \phi_{GeSe-air}^{s(p)} \quad (10)$$

According to the Fresnel equations,[26c] the amplitude reflection coefficient of s-light from the GeSe layer to air $r_{GeSe-air}^{s}$ can be expressed as

$$r_{GeSe-air}^{s} = \frac{N_{AC} - N_{air}}{N_{AC} + N_{air}} \quad (11)$$

where N_{air} (= 1) is the complex refractive index of air. The corresponding amplitude reflection coefficient of the p-light $r_{SnSe-air}^{p}$ is

$$r_{GeSe-air}^{p} = \frac{N_{air} - N_{ZZ}}{N_{air} + N_{ZZ}} \quad (12)$$

Supporting Information

Supporting Information is available from the Wiley Online Library or from the author.

Acknowledgements

Z.G. and H.G. contributed equally to this study. This work was funded by the National Key Research and Development Plan of China (Grant No. 2022YFB2803900), the National Natural Science Foundation of China (Grant Nos. 52130504 and 62125404), the Guangdong Basic and Applied Basic Research Foundation (Grant No. 2023A1515030149), the Key Research and Development Program of Hubei Province (Grant No. 2021BAA013), the Innovation Project of Optics Valley Laboratory (Grant No. OVL2023PY003), and the Fundamental Research Funds for Central Universities (Grant No. 2021XXJS113). The authors are thankful for the support of the Center of Optoelectronic Micro & Nano Fabrication and the Characterizing Facility of the Wuhan National Laboratory of Optoelectronics (WNLO) at Huazhong University of Science and Technology (HUST), the Experiment Center for Advanced Manufacturing and Technology at the School of Mechanical Science & Engineering of HUST, and the Analysis and Testing Center of HUST.

Conflict of Interest

The authors declare no conflict of interest.

Data Availability Statement

Research data are not shared.

© 2024 Wiley-VCH GmbH

Keywords

GeSe, optical anisotropy, optical thin film, perfect absorbers, spectroscopic ellipsometry

Received: December 10, 2023
Revised: March 15, 2024
Published online: April 11, 2024

[1] a) I. E. Khodasevych, L. Wang, A. Mitchell, G. Rosengarten, *Adv. Opt. Mater.* **2015**, *3*, 852; b) K.-T. Lin, H. Lin, T. Yang, B. Jia, *Nat. Commun.* **2020**, *11*, 1389; c) A. Ghobadi, T. G. Ulusoy Ghobadi, F. Karadas, E. Ozbay, *Adv. Opt. Mater.* **2019**, *7*, 1900028.
[2] a) M. Amiri, F. Tofigh, N. Shariati, J. Lipman, M. Abolhasan, *IEEE Internet Things J.* **2021**, *8*, 4105; b) X. Liu, G. Liu, P. Tang, G. Fu, G. Du, Q. Chen, Z. Liu, *Carbon.* **2018**, *140*, 362; c) Y. Yang, K. Kelley, E. Sachet, S. Campione, T. S. Luk, J.-P. Maria, M. B. Sinclair, I. Brener, *Nat. Photonics.* **2017**, *11*, 390.
[3] a) Z. Yang, Y. Chen, Y. Zhou, Y. Wang, P. Dai, X. Zhu, H. Duan, *Adv. Opt. Mater.* **2017**, *5*, 1700029; b) Z. Li, S. Butun, K. Aydin, *ACS Photonics.* **2015**, *2*, 183; c) Z. Xuan, J. Li, Q. Liu, F. Yi, S. Wang, W. Lu, *Innovation.* **2021**, *2*, 100081.
[4] a) S. Kang, Z. Qian, V. Rajaram, S. D. Calisgan, A. Alù, M. Rinaldi, *Adv. Opt. Mater.* **2019**, *7*, 1801236; b) A. Tittl, P. Mai, R. Taubert, D. Dregely, N. Liu, H. Giessen, *Nano Lett.* **2011**, *11*, 4366; c) M. ElKabbash, K. V. Sreekanth, Y. Alapan, M. Kim, J. Cole, A. Fraiwan, T. Letsou, Y. Li, C. Guo, R. M. Sankaran, U. A. Gurkan, M. Hinczewski, G. Strangi, *ACS Photonics.* **2019**, *6*, 1889.
[5] a) N. I. Landy, S. Sajuyigbe, J. J. Mock, D. R. Smith, W. J. Padilla, *Phys. Rev. Lett.* **2008**, *100*, 207402; b) J. Zhou, Z. Liu, X. Liu, G. Fu, G. Liu, J. Chen, C. Wang, H. Zhang, M. Hong, *J. Mater. Chem. C.* **2020**, *8*, 12768; c) C. Ng, L. Wesemann, E. Panchenko, J. Song, T. J. Davis, A. Roberts, D. E. Gómez, *Adv. Opt. Mater.* **2019**, *7*, 1801660.
[6] a) M. Chai, Y. Wang, C. Chen, Z. Zhao, M. Jin, T. He, *Laser Photonics Rev.* **2022**, *16*, 2100458; b) R. Alaee, M. Albooyeh, C. Rockstuhl, *J. Phys. D: Appl. Phys.* **2017**, *50*, 503002; c) G. M. Akselrod, J. Huang, T. B. Hoang, P. T. Bowen, L. Su, D. R. Smith, M. H. Mikkelsen, *Adv. Mater.* **2015**, *27*, 8028.
[7] a) M. A. Kats, R. Blanchard, P. Genevet, F. Capasso, *Nat. Mater.* **2013**, *12*, 20; b) M. A. Kats, F. Capasso, *Laser Photonics Rev.* **2016**, *10*, 735.
[8] a) J. Yang, S. Gurung, S. Bej, P. Ni, H. W. Howard Lee, *Rep. Prog. Phys.* **2022**, *85*, 036101; b) J. Lynch, L. Guarneri, D. Jariwala, J. van de Groep, *J. Appl. Phys.* **2022**, 132; c) B.-X. Wang, C. Xu, G. Duan, W. Xu, F. Pi, *Adv. Funct. Mater.* **2023**, *33*, 2213818.
[9] a) L. Meng, D. Zhao, Q. Li, M. Qiu, *Opt. Express.* **2013**, *21*, A111; b) X. Xiong, Z.-H. Xue, C. Meng, S.-C. Jiang, Y.-H. Hu, R.-W. Peng, M. Wang, *Phys. Rev. B.* **2013**, *88*, 115105; c) W. Fei, X. Jiang, L. Dai, W. Qiu, Y. Fang, D. Li, J. Hu, Q. Zhan, *Opt. Express.* **2023**, *31*, 9608.
[10] a) C. Peng, K. Ou, G. Li, Z. Zhao, X. Li, C. Liu, X. Li, X. Chen, W. Lu, *Opt. Express.* **2021**, *29*, 12893; b) T. Li, B.-Q. Chen, Q. He, L.-A. Bian, X.-J. Shang, G.-F. Song, *Materials.* **2020**, *13*, 5298.
[11] a) Y.-L. Liao, Y. Zhao, *Opt. Quantum Electron.* **2015**, *47*, 2533; b) D. Lee, S. Y. Han, Y. Jeong, D. M. Nguyen, G. Yoon, J. Mun, J. Chae, J. H. Lee, J. G. Ok, G. Y. Jung, H. J. Park, K. Kim, J. Rho, *Sci. Rep.* **2018**, *8*, 12393.
[12] X. Wang, Y. Li, L. Huang, X.-W. Jiang, L. Jiang, H. Dong, Z. Wei, J. Li, W. Hu, *J. Am. Chem. Soc.* **2017**, *139*, 14976.
[13] D. D. Vaughn, R. J. Patel, M. A. Hickner, R. E. Schaak, *J. Am. Chem. Soc.* **2010**, *132*, 15170.
[14] P. A. E. Murgatroyd, M. J. Smiles, C. N. Savory, T. P. Shalvey, J. E. N. Swallow, N. Fleck, C. M. Robertson, F. Jäckel, J. Alaria, J. D. Major, D. O. Scanlon, T. D. Veal, *Chem. Mater.* **2020**, *32*, 3245.
[15] a) S.-C. Liu, Y. Mi, D.-J. Xue, Y.-X. Chen, C. He, X. Liu, J.-S. Hu, L.-J. Wan, *Adv. Electron. Mater.* **2017**, *3*, 1700141; b) J. Tan, Y. Zhao, G. Li, S. Yang, C. Huang, H. Yu, *Adv. Funct. Mater.* **2022**, *32*, 2209094.
[16] X. Hu, P. Huang, K. Liu, B. Jin, X. Zhang, X. Zhang, X. Zhou, T. Zhai, *ACS Appl. Mater. Interfaces.* **2019**, *11*, 23353.
[17] A. Okazaki, *J. Phys. Soc. Jpn.* **1958**, *13*, 1151.
[18] A. Brown, S. Rundqvist, *Acta Crystallogr.* **1965**, *19*, 684.
[19] S. Niu, G. Joe, H. Zhao, Y. Zhou, T. Orvis, H. Huyan, J. Salman, K. Mahalingam, B. Urwin, J. Wu, Y. Liu, T. E. Tiwald, S. B. Cronin, B. M. Howe, M. Mecklenburg, R. Haiges, D. J. Singh, H. Wang, M. A. Kats, J. Ravichandran, *Nat. Photonics.* **2018**, *12*, 392.
[20] J. Qiao, X. Kong, Z.-X. Hu, F. Yang, W. Ji, *Nat. Commun.* **2014**, *5*, 4475.
[21] A. Tołłoczko, S. J. Zelewski, M. Błaszczak, T. Woźniak, A. Siudzińska, A. Bachmatiuk, P. Scharoch, R. Kudrawiec, *J. Mater. Chem. C.* **2021**, *9*, 14838.
[22] Y. Yang, S.-C. Liu, Y. Wang, M. Long, C.-M. Dai, S. Chen, B. Zhang, Z. Sun, Z. Sun, C. Hu, S. Zhang, L. Tong, G. Zhang, D.-J. Xue, J.-S. Hu, *Adv. Opt. Mater.* **2019**, *7*, 1801311.
[23] a) L. Xu, M. Yang, S. J. Wang, Y. P. Feng, *Phys. Rev. B.* **2017**, *95*, 235434; b) M. B. P. Querne, J. M. Bracht, J. L. F. Da Silva, A. Janotti, M. P. Lima, *Phys. Rev. B.* **2023**, *108*, 085409.
[24] a) H. Zhao, Y. Mao, X. Mao, X. Shi, C. Xu, C. Wang, S. Zhang, D. Zhou, *Adv. Funct. Mater.* **2018**, *28*, 1704855; b) H. R. Chandrasekhar, U. Zwick, *Solid State Commun.* **1976**, *18*, 1509.
[25] S. Zhang, S. Liu, S. Huang, B. Cai, M. Xie, L. Qu, Y. Zou, Z. Hu, X. Yu, H. Zeng, *Sci. China Mater.* **2015**, *58*, 929.
[26] a) Z. Guo, H. Gu, M. Fang, B. Song, W. Wang, X. Chen, C. Zhang, H. Jiang, L. Wang, S. Liu, *ACS Mater. Lett.* **2021**, *3*, 525; b) Z. Guo, H. Gu, M. Fang, L. Ye, S. Liu, *Nanoscale.* **2022**, *14*, 12238; c) H. Fujiwara, *Spectroscopic ellipsometry: principles and applications*, John Wiley & Sons, Chichester, England **2007**.
[27] B. Song, H. Gu, S. Zhu, H. Jiang, X. Chen, C. Zhang, S. Liu, *Appl. Surf. Sci.* **2018**, *439*, 1079.
[28] H. Gu, B. Song, M. Fang, Y. Hong, X. Chen, H. Jiang, W. Ren, S. Liu, *Nanoscale.* **2019**, *11*, 22762.
[29] S.-Y. Lee, K.-J. Yee, *2D Mater.* **2021**, *9*, 015020.
[30] H. Yang, H. Jussila, A. Autere, H.-P. Komsa, G. Ye, X. Chen, T. Hasan, Z. Sun, *ACS Photonics.* **2017**, *4*, 3023.
[31] J. C. Manifacier, J. Gasiot, J. P. Fillard, *J. Phys. E: Sci. Instrum.* **1976**, *9*, 1002.
[32] a) W. Shen, C. Hu, S. Huo, Z. Sun, S. Fan, J. Liu, X. Hu, *Opt. Lett.* **2018**, *43*, 1255; b) W. Shen, C. Hu, S. Huo, Z. Sun, G. Fan, J. Liu, L. Sun, X. J. N. Hu, *Nanomaterials.* **2019**, *9*, 168.
[33] Z. Guo, H. Gu, Y. Yu, Z. Wei, S. Liu, *Nanomaterials.* **2023**, *13*, 134.
[34] J.-H. Kim, S.-Y. Jung, I.-K. Jeong, *J. Opt. Soc. Korea.* **2012**, *16*, 6.
[35] R. Gopal, K. Poopathy, R. Ganesan, E. Thangavel, k. B Arjun, M. Nadarajah, K. Kaviyarasu, in *Quantum Dots: Fundamental and Applications*, (Ed: D. Faten), IntechOpen, Rijeka **2020**, Ch 2.
[36] C. Wei, S. Abedini Dereshgi, X. Song, A. Murthy, V. P. Dravid, T. Cao, K. Aydin, *Adv. Opt. Mater.* **2020**, *8*, 2000088.
[37] A. Tudi, S. Han, Z. Yang, S. Pan, *Coord. Chem. Rev.* **2022**, *459*, 214380.
[38] M. A. Kats, F. Capasso, *Laser Photonics Rev.* **2016**, *10*, 735.

© 2024 Wiley-VCH GmbH

ADVANCED OPTICAL MATERIALS

Supporting Information

for *Adv. Optical Mater.*, DOI 10.1002/adom.202303138

Wavelength-Linearly-Dependent and Polarization-Sensitive Perfect Absorbers based on Optically Anisotropic Germanium Selenide (GeSe)

Zhengfeng Guo, Honggang Gu, Yali Yu, Qihang Zhang, Zhongming Wei* and Shiyuan Liu**

Supporting Information for

Wavelength-Linearly-Dependent and Polarization-Sensitive Perfect Absorbers based on Optically Anisotropic Germanium Selenide (GeSe)

Zhengfeng Guo[1,2,#], *Honggang Gu*[1,3,4,#,*], *Yali Yu*[5], *Qihang Zhang*[1], *Zhongming Wei*[5,*], *and Shiyuan Liu*[1,4,6,*]

[1] State Key Laboratory of Intelligent Manufacturing Equipment and Technology, Huazhong University of Science and Technology (HUST), Wuhan 430074, China

[2] Innovation Institute, Huazhong University of Science and Technology, Wuhan 430074, China

[3] Guangdong HUST Industrial Technology Research Institute, Guangdong Provincial Key Laboratory of Manufacturing Equipment Digitization, Dongguan, Guangdong 523003, China

[4] Optics Valley Laboratory, Hubei 430074, China

[5] State Key Laboratory of Superlattices and Microstructures, Institute of Semiconductors, Chinese Academy of Sciences, Beijing 100083, China

[6] School of Optical and Electronic Information, Huazhong University of Science and Technology, Wuhan 430074, China

[#] These authors contribute equally to this work

* Corresponding E-mails: hongganggu@hust.edu.cn (H. G.); zmwei@semi.ac.cn (Z. W.); shyliu@hust.edu.cn (S. L.)

Index

Section S1. Optical Anisotropy of GeSe 3

S1.1 Typical morphology of exfoliated GeSe nanosheet 3

S1.2 Mueller matrix spectroscopic ellipsometric measurement and analysis 3

S1.3 Relation between the dielectric tensor and the complex refractive index tensor 6

Section S2. Wavelength-Linearly-Dependent Perfect Absorber Modulated by Layer Thicknesses 7

S2.1 Optimizing thickness of the GeSe layer and the SiO_2 layer 7

S2.2 Distribution of electric field intensity *I* spectra and power dissipation *Q* spectra 14

Section S3. Polarization-Sensitive Reconfigurable Perfect Absorbers 16

S3.1 Theoretical derivation of the relation between the absorbance *Abs* and the polarization angle α 16

S3.2 Linear relationship between operating wavelength and GeSe thickness 18

S3.3 Experimentally Confirming Polarization-Sensitive Reconfigurable Perfect Absorber 20

Reference 22

Section S1. Optical Anisotropy of GeSe

S1.1 Typical morphology of exfoliated GeSe nanosheet

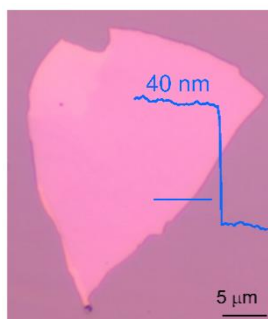

Figure S1. The typical morphology of exfoliated GeSe nanosheet with whose thickness measured by the atomic force microscope (AFM).

S1.2 Mueller matrix spectroscopic ellipsometric measurement and analysis

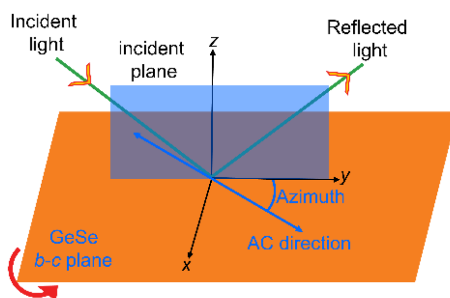

Figure S2. Ellipsometric measurement schematic diagram of GeSe single crystal sample, where the azimuth is defined as the angle between AC direction of GeSe and y-axis of ellipsometric coordinate (x-y-z).

Supporting Note S1. Mueller matrix spectroscopic ellipsometric analysis

In the Mueller matrix spectroscopic ellipsometry analysis, the simulated Mueller matrix spectra calculated by the constructed and optimized optical model are utilized to well match the experimental ones. Herein, the optical model is composed of not only the geometric structure but also the corresponding dielectric tensor. For the GeSe single crystal sample, its geometric structure can be regard as the anisotropic substrate without considering roughness or overlay model (such as effective medium approximation, EMA[1]). Since GeSe's low-symmetry structure belongs to the orthorhombic crystal system, its dielectric tensor is diagonal and the elements of the dielectric tensor, namely dielectric functions, are along the GeSe's crystal axes, which is ε_a, ε_b, and ε_c. In Figure S2a, we denote ε_b and ε_c as $\varepsilon_{\mathrm{ZZ}}$ and $\varepsilon_{\mathrm{AC}}$ respectively as *b*- and *c*-axis of GeSe can be also regarded as zigzag (ZZ) and armchair (AC) direction respectively. To acquire the dielectric tensor of this anisotropic substrate, the Tauc-Lorentz oscillators have been adopted along the *b*- and *c*-axis of GeSe while the Cauchy model has employed in view of the van der Waals (vdW) interactions along the *a*-axis.[2] The dielectric functions along the ZZ and AC direction, *i.e.* $\varepsilon_{\mathrm{ZZ}}$ and $\varepsilon_{\mathrm{AC}}$, can be represented as the sum of several Tauc-Lorentz oscillators[3]

$$\varepsilon_m(E)=\sum_{q}^{Q}\varepsilon_{\text{Tauc-Lorentz}}^{q}(A_q,\eta_q,E_{0,\,q},E_{\mathrm{g},\,q};E),\ m=\mathrm{ZZ}\text{ and AC}. \tag{S1}$$

In Equation S1, E is the photon energy with the unit of eV, Q is the total number of oscillators, and A_q, η_q, $E_{0,\,q}$, and $E_{\mathrm{g},\,q}$ are the qth oscillator's amplitude, damping coefficient, peak transition energy, and bandgap energy respectively. And the qth Tauc-Lorentz oscillator consists of the real part $\varepsilon_{\mathrm{r},\,q}$ and the imaginary part $\varepsilon_{\mathrm{i},\,q}$ in Equation S2a

$$\varepsilon_{\text{Tauc-Lorentz}}^{q}(E)=\varepsilon_{\mathrm{r},\,q}(E)+\mathrm{i}\varepsilon_{\mathrm{i},\,q}(E), \tag{S2a}$$

where $\varepsilon_{\mathrm{i},\,q}$ can be expressed as[3]

$$\varepsilon_{\mathrm{i},\,q}(E)=\begin{cases}\dfrac{A_q\eta_q E_{0,\,q}(E-E_{\mathrm{g},\,q})^2}{(E^2-E_{0,\,q}^2)^2+\eta_q^2E^2}\cdot\dfrac{1}{E}; & E>E_{\mathrm{g},\,q}\\ 0. & E\le E_{\mathrm{g},\,q}\end{cases} \tag{S2b}$$

and $\varepsilon_{\mathrm{r},\,q}$ can be converted from $\varepsilon_{\mathrm{i},\,q}$ by the Kramers–Kronig relation[3b] of Equation S2c

$$\varepsilon_{r,q}(E) = \varepsilon_{r,q}(\infty) + \frac{2}{\pi} P \int_{E_{g,q}}^{\infty} \frac{\xi \varepsilon_{i,q}(\xi)}{\xi^2 - E^2} d\xi . \quad \text{(S2c)}$$

The dielectric function along a-axis ε_a is described by the Cauchy model,[2, 3b] which is defined by the refractive index n and the extinction coefficient k in Equation S3

$$n(E) = A + BE^2 + CE^4;\ k = 0 , \quad \text{(S3)}$$

where A, B, and C represent the analytical parameters of the Cauchy model. Besides, the Euler angles ψ and θ are introduced to make the crystal axes parallel to the ellipsometric coordinate axes.

To obtain the optimal dielectric tensor of GeSe, both three Tauc-Lorentz oscillators have been selected to model the ε_{ZZ} and ε_{AC}, whose best fitted parameters are listed in Table S1. As to ε_a, the A, B, and C of corresponding Cauchy model are respectively 1.31, 8.02×10^{-3}, and 3.06×10^{-4}. Besides, the optimized Euler angles ψ and θ are respectively 40.09° and −2.21°. Finally, we have acquired the optimal dielectric tensor of GeSe as illustrated in Figure 2a.

Table S1. The best fitted parameters of Tauc-Lorentz oscillators along the ZZ and AC direction of GeSe.

Dielectric functions ε	Peak transition energy E_0 [eV]	Amplitude A [eV]	Damping coefficient η [eV]	Bandgap energy E_g [eV]
ε_{ZZ}	2.32	79.921	1.35	1.45
	3.67	23.49	3.38	0.28
	5.00	122.39	1.37	5.31
ε_{AC}	1.39	87.02	1.02	1.35
	3.50	26.02	2.31	0.29
	3.63	114.49	8.75	5.31

S1.3 Relation between the dielectric tensor and the complex refractive index tensor

Supporting Note S2. Converting the dielectric tensor into the complex refractive index tensor

GeSe's dielectric tensor and complex refractive index tensor can be mutually converted by Equation S4[4]

$$\begin{bmatrix} \varepsilon_a & 0 & 0 \\ 0 & \varepsilon_b & 0 \\ 0 & 0 & \varepsilon_c \end{bmatrix} = \begin{bmatrix} N_a^2 & 0 & 0 \\ 0 & N_b^2 & 0 \\ 0 & 0 & N_c^2 \end{bmatrix}, \tag{S4a}$$

where the subscript *a*, *b*, and *c* denote the dielectric functions ε and the complex refractive indexes *N* along the *a*-, *b*-, and *c*-axis of GeSe respectively.

Besides, the dielectric function ε is composed of real part ε_r and imaginary part ε_i, *i.e.* $\varepsilon = \varepsilon_r + \mathrm{i}\varepsilon_i$, while the refractive index *n* and the extinction coefficient *k* constitute the complex refractive index N $(= n + \mathrm{i}k)$. Therefore, the Equation S4a can be further expressed as

$$\begin{bmatrix} \varepsilon_{\mathrm{r},a} + \mathrm{i}\varepsilon_{\mathrm{i},a} & 0 & 0 \\ 0 & \varepsilon_{\mathrm{r},b} + \mathrm{i}\varepsilon_{\mathrm{i},b} & 0 \\ 0 & 0 & \varepsilon_{\mathrm{r},c} + \mathrm{i}\varepsilon_{\mathrm{i},c} \end{bmatrix} = \begin{bmatrix} (n_a + \mathrm{i}k_a)^2 & 0 & 0 \\ 0 & (n_b + \mathrm{i}k_b)^2 & 0 \\ 0 & 0 & (n_c + \mathrm{i}k_c)^2 \end{bmatrix}. \tag{S4b}$$

Here, the detailed description of the complex refractive index by the real and imaginary part of dielectric function can be further given

$$n_j = \sqrt{\frac{\varepsilon_{\mathrm{r},j} + \sqrt{\varepsilon_{\mathrm{r},j}^2 + \varepsilon_{\mathrm{i},j}^2}}{2}},\ j = a,\ b,\ c; \tag{S5a}$$

$$k_j = \sqrt{\frac{-\varepsilon_{\mathrm{r},j} + \sqrt{\varepsilon_{\mathrm{r},j}^2 + \varepsilon_{\mathrm{i},j}^2}}{2}},\ j = a,\ b,\ c. \tag{S5b}$$

Section S2. Wavelength-Linearly-Dependent Perfect Absorber Modulated by Layer Thicknesses

S2.1 Optimizing thickness of the GeSe layer and the SiO_2 layer

Supporting Note S3. The destructive interference condition of multilayered optical thin film like GeSe-SiO_2-Si structure

As is known, the destructive interference condition is a phase retardation of $m\pi/2$ between two electromagnetic waves. However, the situation becomes much more complicated when it comes to the destructive interference condition of multilayered optical thin film like GeSe-SiO_2-Si structure. The destructive interference comes from optical path difference caused by not only the multiple reflections and transmissions at the interface of both air-GeSe and GeSe-SiO_2 but also the reflections at the interface of SiO_2-Si. Therefore, the net phase shift is selected to calculate the destructive interference condition, which is feasible and computable.

According to the Equation 3 in the manuscript, the destructive interference can be realized when Reflectance of p- and s-light (R_p and R_s) are zero, which means the the absorbance of p- or s-light (Abs_p or Abs_s) rearch unity, *i.e.* perfect absorption. As is known, the R_p and R_s of GeSe-SiO_2-Si multilayered optical thin film can be calculated from the amplitude reflection coefficient $r^{s(p)}_{\text{air-GeSe-SiO}_2\text{-Si}}$, which is[3b]

$$R_{s(p)} = \left| r^{s(p)}_{\text{air-GeSe-SiO}_2\text{-Si}} \right|^2 = \left| \frac{r^{s(p)}_{\text{air-GeSe}} + r^{s(p)}_{\text{GeSe-SiO}_2\text{-Si}} \exp(\mathrm{i}2\beta^{s(p)}_{\text{GeSe}})}{1 + r^{s(p)}_{\text{air-GeSe}} r^{s(p)}_{\text{GeSe-SiO}_2\text{-Si}} \exp(\mathrm{i}2\beta^{s(p)}_{\text{GeSe}})} \right|^2 . \tag{S6}$$

In Equation S6, $r^{s(p)}_{\text{air-GeSe}}$ and $r^{s(p)}_{\text{GeSe-SiO}_2\text{-Si}}$ are respectively the amplitude reflection coefficient of s-(p-)light for air-GeSe structure and GeSe-SiO_2-Si structure. Besides, the phase variation of GeSe layer $\beta^{s(p)}_{\text{GeSe}}$ is given by $\beta^{s(p)}_{\text{GeSe}} = 2\pi d_{\text{GeSe}} N_{\text{AC(ZZ)}} / \lambda$ as the vibrational directions of s- and p-light keep parallel to the AC and ZZ directions of GeSe respectively at normal incidence all the time. To make R_p and R_s become zero, the numerator in Equation S6 should be zero, which is

$$r^{s(p)}_{\text{air-GeSe}} + r^{s(p)}_{\text{GeSe-SiO}_2\text{-Si}} \exp(\mathrm{i}2\beta^{s(p)}_{\text{GeSe}}) = 0. \tag{S7}$$

According to Fresnel equations[3b], s-light's amplitude reflection coefficient from air to GeSe layer $r^{\mathrm{s}}_{\text{air-GeSe}}$ can be expressed as[3b]

$$r^{\mathrm{s}}_{\text{air-GeSe}}=\frac{N_{\mathrm{air}}-N_{\mathrm{AC}}}{N_{\mathrm{air}}+N_{\mathrm{AC}}}, \tag{S8a}$$

where N_{air} (= 1) is the complex refractive index of air. The corresponding amplitude reflection coefficient of p-light $r^{\mathrm{p}}_{\text{air-GeSe}}$ is represented as[3b]

$$r^{\mathrm{p}}_{\text{air-GeSe}}=\frac{N_{ZZ}-N_{\mathrm{air}}}{N_{ZZ}+N_{\mathrm{air}}}. \tag{S8b}$$

Compared with the Equation 9 and 10 in the main text, the amplitude reflection coefficients from GeSe layer to air $r^{\mathrm{s(p)}}_{\text{GeSe-air}}$ have the following relation with those from air to GeSe layer $r^{\mathrm{s(p)}}_{\text{air-GeSe}}$

$$r^{\mathrm{s(p)}}_{\text{GeSe-air}}=-\,r^{\mathrm{s(p)}}_{\text{air-GeSe}}. \tag{S9}$$

As a consequence, Equation S7 can be rewritten as

$$r^{\mathrm{s(p)}}_{\text{GeSe-SiO}_2\text{-Si}}\exp(\mathrm{i}2\beta^{\mathrm{s(p)}}_{\mathrm{GeSe}})=-r^{\mathrm{s(p)}}_{\text{air-GeSe}}=r^{\mathrm{s(p)}}_{\text{GeSe-air}}, \tag{S10a}$$

which can be further expanded as

$$\left|r^{\mathrm{s(p)}}_{\text{GeSe-SiO}_2\text{-Si}}\right|\exp(\mathrm{i}\,\phi^{\mathrm{s(p)}}_{\text{GeSe-SiO}_2\text{-Si}})\exp(\mathrm{i}\frac{4\pi d_{\mathrm{GeSe}}N_{\mathrm{AC(ZZ)}}}{\lambda})=\left|r^{\mathrm{s(p)}}_{\text{GeSe-air}}\right|\exp(\mathrm{i}\,\phi^{\mathrm{s(p)}}_{\text{GeSe-air}}). \tag{S10b}$$

In Equation S10b, $\phi^{\mathrm{s(p)}}_{\text{GeSe-SiO}_2\text{-Si}}$ and $\phi^{\mathrm{s(p)}}_{\text{GeSe-air}}$ are the arguments of corresponding amplitude reflection coefficient, and we also take $\beta^{\mathrm{s(p)}}_{\mathrm{GeSe}}=2\pi d_{\mathrm{GeSe}}N_{\mathrm{AC(ZZ)}}/\lambda$ into Equation S10a.

To obtain Equation S10, *i.e.* perfect absorption, an amplitude condition and a phase condition must be satisfied at the same time.[5] The amplitude condition is[5]

$$\left|r^{\mathrm{s(p)}}_{\text{GeSe-air}}\right|=\left|r^{\mathrm{s(p)}}_{\text{GeSe-SiO}_2\text{-Si}}\right|\exp(-\frac{4\pi d_{\mathrm{GeSe}}k_{\mathrm{AC(ZZ)}}}{\lambda})=\left|r^{\mathrm{s(p)}}_{\text{GeSe-SiO}_2\text{-Si}}\right|\exp(-d_{\mathrm{GeSe}}\alpha_{\mathrm{AC(ZZ)}}), \tag{S11}$$

where $\alpha_{\mathrm{AC(ZZ)}}$ is the absorption coefficients along the AC(ZZ) direction of GeSe. Take Equation S11 into the right side of Equation S10b, the Equation S10b can be consequently reduced the $\left|r^{\mathrm{s(p)}}_{\text{GeSe-SiO}_2\text{-Si}}\right|$, which is

$$\exp\left\{\mathrm{i}\left[\phi^{\mathrm{s(p)}}_{\text{GeSe-SiO}_2\text{-Si}}+\frac{4\pi d_{\mathrm{GeSe}}(n_{\mathrm{AC(ZZ)}}+\mathrm{i}\,k_{\mathrm{AC(ZZ)}})}{\lambda}\right]\right\}=\exp(\mathrm{i}\,\phi^{\mathrm{s(p)}}_{\text{GeSe-air}}-\frac{4\pi d_{\mathrm{GeSe}}k_{\mathrm{AC(ZZ)}}}{\lambda}). \quad \text{(S12a)}$$

Here, we use the equation of $N_{\mathrm{AC(ZZ)}} = n_{\mathrm{AC(ZZ)}} + \mathrm{i}k_{\mathrm{AC(ZZ)}}$. After simplification, Equation S12a can be equivalent to

$$\exp\left[\mathrm{i}(\phi^{\mathrm{s(p)}}_{\text{GeSe-SiO}_2\text{-Si}}+\frac{4\pi d_{\mathrm{GeSe}}n_{\mathrm{AC(ZZ)}}}{\lambda}-\phi^{\mathrm{s(p)}}_{\text{GeSe-air}})\right]=1=\exp(\mathrm{i}\,2\pi m), \quad \text{(S12b)}$$

where m is an integer.

Here, we define the net phase shift $\phi^{\mathrm{s(p)}}_{\mathrm{net}}$ as

$$\phi^{\mathrm{s(p)}}_{\mathrm{net}}=\phi^{\mathrm{s(p)}}_{\text{GeSe-SiO}_2\text{-Si}}+\frac{4\pi d_{\mathrm{GeSe}}n_{\mathrm{AC(ZZ)}}}{\lambda}-\phi^{\mathrm{s(p)}}_{\text{GeSe-air}}. \quad \text{(S13)}$$

Therefore, the destructive interference condition, also the phase condition, can be ultimately obtained

$$\phi^{\mathrm{s(p)}}_{\mathrm{net}}=\phi^{\mathrm{s(p)}}_{\text{GeSe-SiO}_2\text{-Si}}+\frac{4\pi d_{\mathrm{GeSe}}n_{\mathrm{AC(ZZ)}}}{\lambda}-\phi^{\mathrm{s(p)}}_{\text{GeSe-air}}=2\pi m. \quad \text{(S14)}$$

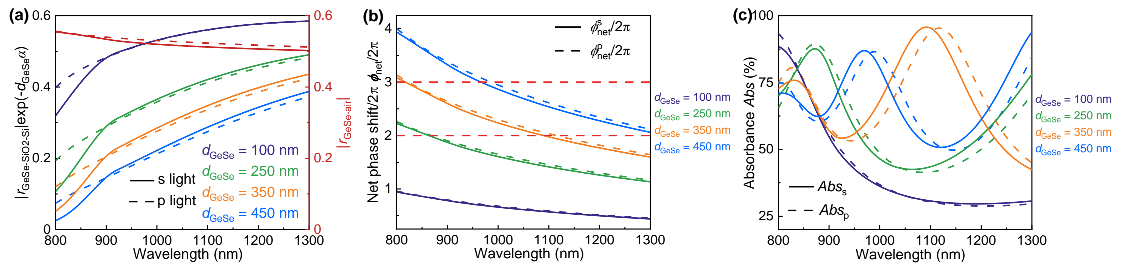

Figure S3. a) amplitude condition of perfect absorption, b) Net phase shift/2π $\phi_{\mathrm{net}}/2\pi$, and c) absorbance *Abs* spectra for both s- and p-light varied with the d_{GeSe} of 100, 250, 350, and 450 nm.

Supporting Note S4. Selecting optimal thickness of SiO_2 layer

The bright and shaded stripes alternately emerge in both Abs_s and Abs_p spectra of Figure S7a and Figure S7b with the increase of d_{SiO_2} due to the interference effect of multilayered optical thin film.[6] Considering the lossless dielectric feature of SiO_2, the maximum of Abs_s and Abs_p remain unchanged with the increase of d_{SiO_2}, which is consistent with the circumstance of Figure S5b. With the increase of d_{SiO_2}, we mark region A, B, and C of nearly perfect absorption ($Abs > 96\%$) for both Abs_s and Abs_p.

We have also calculated other contour maps of Abs_s and Abs_p varied with the d_{SiO_2} with the d_{GeSe} of 150, 175, and 200 nm, and their region A, B, and C are listed in Table S2. To realize the possible perfect absorption, we screen the d_{SiO_2} region to simultaneously satisfy the criterion of $Abs > 96\%$ for both Abs_s and Abs_p, which is 156−245 nm for region A, 479−563 nm for region B, and 869−885 nm for region C. Therefore, it is reasonable to select middle thickness of the longest region, *i.e.* 200 nm in region A, to obtain the probable perfect absorbers in consideration of adaptability and easy frabrication.

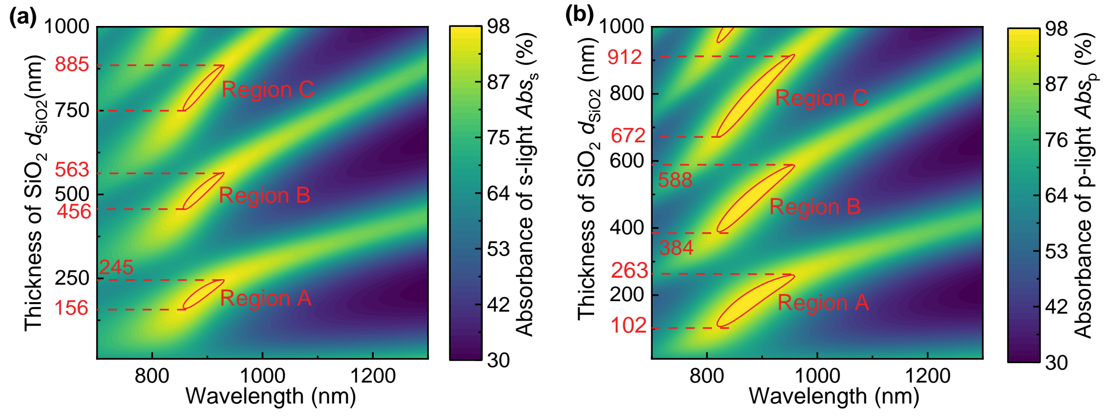

Figure S4. Contour maps of a) Abs_s and b) Abs_p spectra varied with the d_{SiO_2} when the d_{GeSe} is 125 nm.

Table S2. Region A, B, and C of nearly perfect absorption (Abs > 96%) with the d_{GeSe} of 125, 150, 175, and 200 nm.

d_{GeSe} [nm]	Region A for s-light [nm]	Region A for p-light [nm]	Region B for s-light [nm]	Region B for p-light [nm]	Region C for s-light [nm]	Region C for p-light [nm]
125	156−245	102−263	456−563	384−588	750−885	672−912
150	95−317	93−315	409−704	414−706	719−1000	731−1000
175	91−376	91−376	438−781	444−795	816−1000	820−1000
200	87−338	87−317	462−778	479−672	842−1000	869−1000

Supporting Note S5. The influence of the thickness of Si to the perfect absorption

Owing to quite thin thickness of Si layer, the p- and s-light's transmittance T_p and T_s are incapable of being ignored. Therefore, the Abs_p and Abs_s can be calculated from the equation below

$$Abs_j = 1 - R_j - T_j,\ j = \text{s or p.} \tag{S15}$$

Illustrated in Figure S5a and 5b, we have calculated the absorbance of p- and s-light (Abs_p and Abs_s) varied with the thickness of silica (Si), and the thicknesses of GeSe and SiO_2 are fixed at 150 and 200 nm respectively. The operating wavelength of GeSe-SiO_2-Si multilayered optical thin film keeps nearly unchanged with the increase of the thickness of Si for both p- and s-light.

According to the complex refractive index of Si substrate measured by the ellipsometry in Figure S5c, the Si shows the rather weak absorption like GeSe since the extinction coefficient k gradually reduces to zero. Such weak absorption feature of Si will also bring the interference effect with the variation of its thickness, which demonstrated by the alternately arranged bright and shaded stripes in both Abs_p and Abs_s spectra of Figure S5a and Sb. One can also observe this interference effect from Figure S5d as both the p-(s-)light's absorbance $Abs_{p(s)}$ and its transmittance $T_{p(s)}$ oscillate with the increase of the thickness of Si.

Since the extinction coefficient k of Si is two orders of magnitude smaller than that of GeSe, the T_p and T_s still keep a range from about 20% to about 50% with the increase of the thickness of Si in Figure S5d. When the thickness of Si increases to scale of micrometers and finally reaches to 1 mm in Figure S5e and 5f, the T_p and T_s as well as Reflectance of p- and s-light R_p and R_s gradually decrease to zero and Abs_p and Abs_s approach to 100%. Therefore, it is of great necessity to select Si as the substrate to realize perfect absorption.

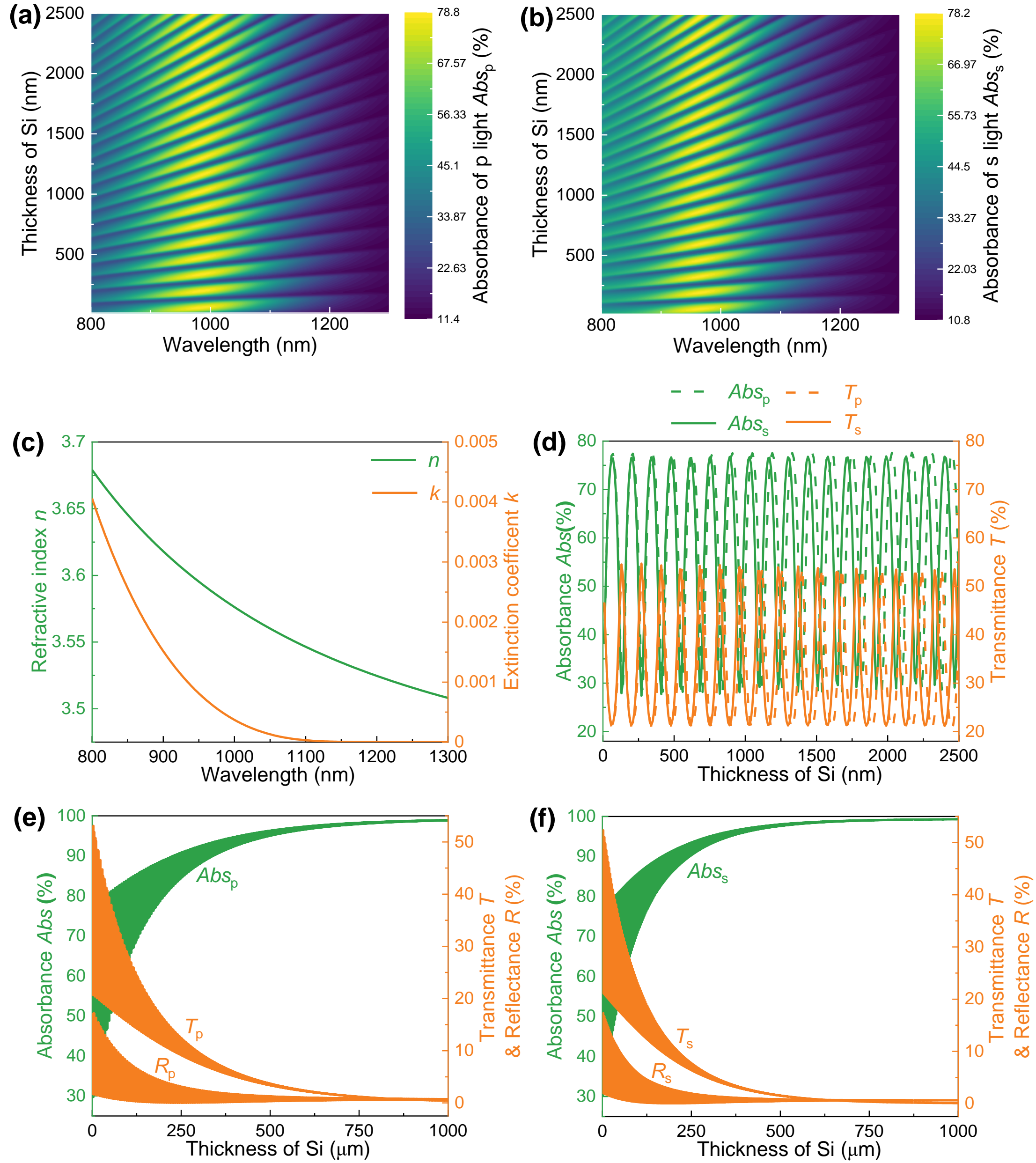

Figure S5. The influence of the thickness of Si to the perfect absorption. The absorbance of p- and s-light a) Abs_p and b) Abs_s varied with the thickness of Si, and the thicknesses of GeSe and SiO_2 are fixed at 150 and 200 nm respectively. c) The complex refractive index of Si substrate measured by the ellipsometry. d) The p- and s-light's absorbance Abs_p and Abs_s and transmittance T_p and T_s varied with the thickness of Si at their operating wavelengths (1003 nm for p- light and 985 nm for s-light) and the same thickness of GeSe and SiO2 (150 and 200 nm respectively).The absorbance, and transmittance as well as Reflectance for e) p- and f) s-light with the much thicker thickness of Si at the same operating wavelengths and the same thickness of GeSe and SiO_2 as those of d).

S2.2 Distribution of electric field intensity *I* spectra and power dissipation *Q* spectra

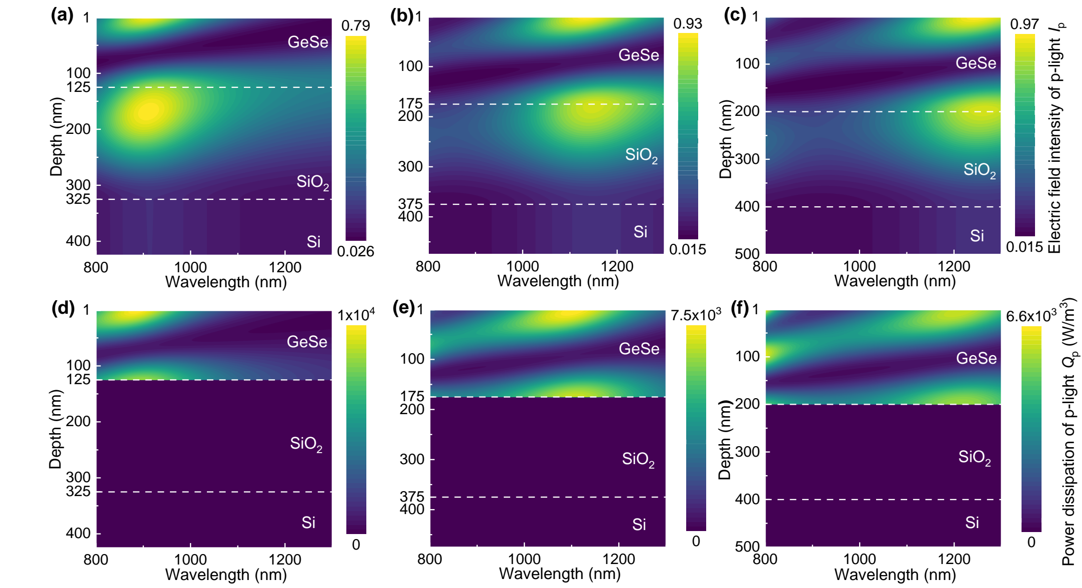

Figure S6. Distribution of a/b/c) p-light's electric field intensity I_p spectra and d/e/f) power dissipation Q_p spectra of GeSe based optical thin film at the d_{GeSe} of 150/175/200 nm.

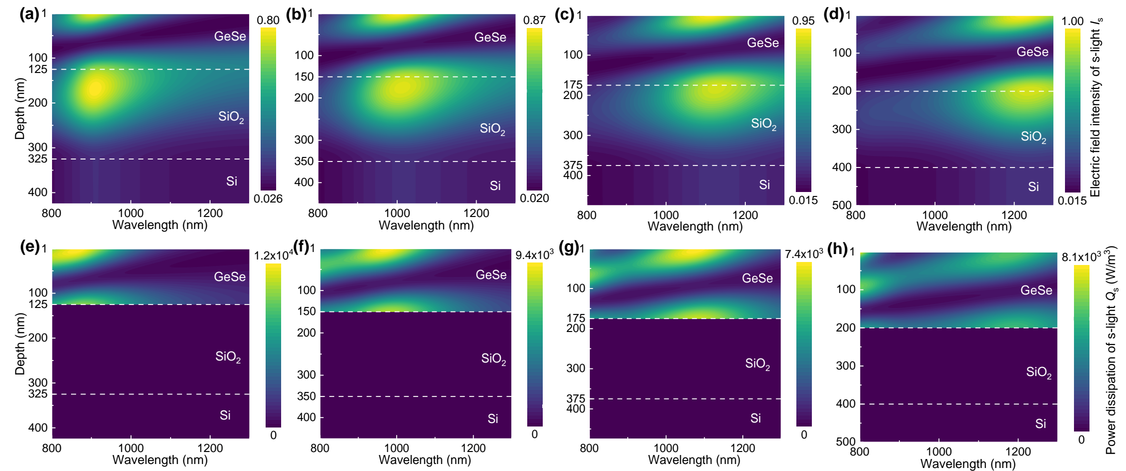

Figure S7. Distribution of a/b/c/d) s-light's electric field intensity I_s spectra and e/f/g/h) power dissipation Q_s spectra of GeSe based optical thin film at the d_{GeSe} of 125/150/175/200 nm.

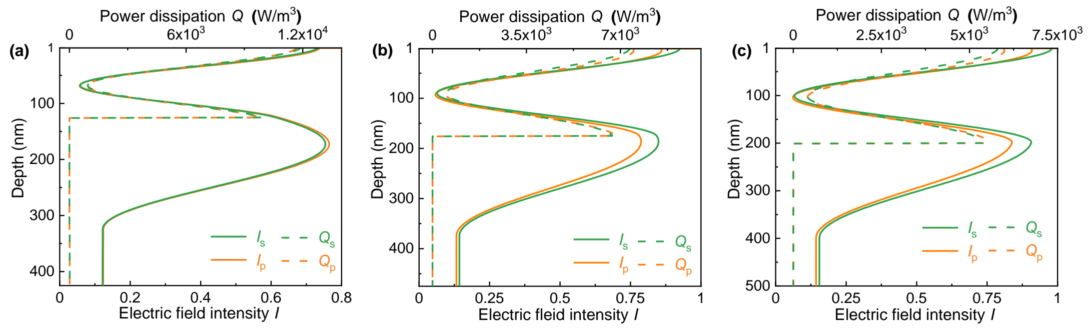

Figure S8. a/b/c) Distribution of electric field intensity *I* spectra and power dissipation *Q* spectra for both s- and p-light at the different d_{GeSe} (125/175/200 nm) and their perfect absorption wavelength.

Section S3. Polarization-Sensitive Reconfigurable Perfect Absorbers

S3.1 Theoretical derivation of the relation between the absorbance *Abs* and the polarization angle α

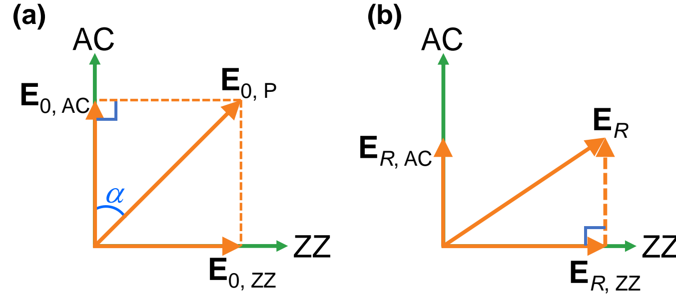

Figure S9. a) The electric field after going through the polarizer $\mathbf{E}_{0,\ \mathrm{p}}$ with its decomposed electric field component along the AC and ZZ direction, *i.e.* $\mathbf{E}_{0,\ \mathrm{AC}}$ and $\mathbf{E}_{0,\ \mathrm{ZZ}}$, where the polarization angle α is defined as the angle between the vertical direction (the AC direction) and $\mathbf{E}_{0,\ \mathrm{p}}$. b) The refelcted electric field $\mathbf{E}_{\mathrm{R}}$, the refelcted electric field along AC direction $\mathbf{E}_{\mathrm{R},\ \mathrm{AC}}$, and the refelcted electric field along AC direction $\mathbf{E}_{\mathrm{R},\ \mathrm{ZZ}}$ form a right triangle, where $\mathbf{E}_{\mathrm{R}}$ is the hypotenuse and $\mathbf{E}_{\mathrm{R},\ \mathrm{AC}}$ and $\mathbf{E}_{\mathrm{R},\ \mathrm{ZZ}}$ are the right-angle sides.

Supporting Note S6. The relation between the absorbance *Abs* and the polarization angle α

The electric field after going through the polarizer of Figure 2a, $\mathbf{E}_{0,\ \mathrm{p}}$, can be decomposed into the electric field component along the AC and ZZ direction, *i.e.* $\mathbf{E}_{0,\ \mathrm{AC}}$ and $\mathbf{E}_{0,\ \mathrm{ZZ}}$, with following relation

$$E_{0,\ \mathrm{AC}} = E_{0,\ \mathrm{P}} \cos\alpha \tag{S16a}$$

$$E_{0,\ \mathrm{ZZ}} = E_{0,\ \mathrm{P}} \sin\alpha \tag{S16b}$$

In Equation S16, α is the polarization angle,which is defined as the the angle between the vertical direction (the AC direction) and $\mathbf{E}_{0,\ \mathrm{p}}$ in Figure S9a.

The amplitude reflection coefficient along the AC and ZZ direction r_{AC} and r_{ZZ} respectively connect $\mathbf{E}_{0,\ \mathrm{AC}}$ and $\mathbf{E}_{0,\ \mathrm{ZZ}}$ with the refelcted electric field along AC and ZZ direction $\mathbf{E}_{\mathrm{R},\ \mathrm{AC}}$ and $\mathbf{E}_{\mathrm{R},\ \mathrm{ZZ}}$ in Equation S8

$$r_{\mathrm{AC}} = \frac{E_{R,\ \mathrm{AC}}}{E_{0,\ \mathrm{AC}}} \tag{S17a}$$

$$r_{\mathrm{ZZ}} = \frac{E_{R,\ \mathrm{ZZ}}}{E_{0,\ \mathrm{ZZ}}} \tag{S17b}$$

According to Equation S16 and S17, the $\mathbf{E}_{\mathrm{R,\ AC}}$ and $\mathbf{E}_{\mathrm{R,\ ZZ}}$ can be expressed as

$$E_{R,\ \mathrm{AC}} = r_{\mathrm{AC}} E_{0,\ \mathrm{AC}} = r_{\mathrm{AC}} E_{0,\ \mathrm{P}} \cos\alpha \tag{S18a}$$

$$E_{R,\ \mathrm{ZZ}} = r_{\mathrm{ZZ}} E_{0,\ \mathrm{ZZ}} = r_{\mathrm{ZZ}} E_{0,\ \mathrm{P}} \sin\alpha \tag{S18b}$$

As shown in Figure S9b, the refelcted electric field $\mathbf{E}_{\mathrm{R}}$, $\mathbf{E}_{\mathrm{R,\ AC}}$, and $\mathbf{E}_{\mathrm{R,\ ZZ}}$ form a right triangle, where $\mathbf{E}_{\mathrm{R}}$ is the hypotenuse and $\mathbf{E}_{\mathrm{R,\ AC}}$ and $\mathbf{E}_{\mathrm{R,\ ZZ}}$ are the right-angle sides. Therefore, the relation between the refectance R and the polarization angle α can be expressed as

$$\begin{aligned} R(\alpha) &= \left|\frac{E_R}{E_{0,\ \mathrm{P}}}\right|^2 = \frac{\left|\sqrt{E_{R,\ \mathrm{AC}}^2 + E_{R,\ \mathrm{ZZ}}^2}\right|^2}{\left|E_{0,\ \mathrm{P}}\right|^2} \\ &= \left|r_{\mathrm{AC}}\right|^2 \cos^2\alpha + \left|r_{\mathrm{ZZ}}\right|^2 \sin^2\alpha \\ &= R_{\mathrm{AC}} \cos^2\alpha + R_{\mathrm{ZZ}} \sin^2\alpha \end{aligned} \tag{S19}$$

Since the vibrational directions of the s- and p-light always keep parallel to the AC and ZZ directions of GeSe respectively at normal incidence, Equation S19 can be rewrited as

$$R(\alpha) = R_{\mathrm{s}} \cos^2\alpha + R_{\mathrm{p}} \sin^2\alpha \tag{S20}$$

Ultimately, the relation between the absorbance Abs and the polarization angle α is denoted as

$$\begin{aligned} Abs(\alpha) &= 1 - R(\alpha) \\ &= 1 - R_{\mathrm{s}} \cos^2\alpha - R_{\mathrm{p}} \sin^2\alpha \end{aligned} \tag{S21}$$

S3.2 Linear relationship between operating wavelength and GeSe thickness

Supporting Note S7. Explanations about the linear relationship between operating wavelength and GeSe thickness

As shown in Figure 3b of manuscript, the wavelengths corresponding to the net phase shift ϕ_{net} of 2π for both s- or p-light are equal to those of $Abs_{\text{s, max}}$ and $Abs_{\text{p, max}}$, *i.e.* the operating wavelength λ_{ope}. Therefore, the operating wavelength λ_{ope} have the following relation with the thickness of GeSe d_{GeSe}, according to the phase condition of perfect absorption

$$\phi_{\text{net}}^{\text{s(p)}} = \phi_{\text{GeSe-SiO}_2\text{-Si}}^{\text{s(p)}} + \frac{4\pi d_{\text{GeSe}} n_{\text{AC(ZZ)}}}{\lambda} - \phi_{\text{GeSe-air}}^{\text{s(p)}} = 2\pi. \tag{S22}$$

Equation S22 can be further converted as

$$\lambda_{\text{ope}} = \frac{4\pi n_{\text{AC(ZZ)}}}{2\pi + \phi_{\text{GeSe-air}}^{\text{s(p)}} - \phi_{\text{GeSe-SiO}_2\text{-Si}}^{\text{s(p)}}} d_{\text{GeSe}}, \tag{S23}$$

where $\phi_{\text{GeSe-air}}^{\text{s (p)}}$ and $\phi_{\text{GeSe-SiO}_2\text{-Si}}^{\text{s (p)}}$ are respectively the s-(p-)light's argument of the corrsponding amplitude reflection coefficient for air-GeSe structure and GeSe-SiO_2-Si structure. If the operating wavelength λ_{ope} appears to be linear with the thickness of GeSe d_{GeSe}, the denominator and the numerator of Equation S23 should have the similar even almost the same variation tendency.

As dmonstrated in Figure S10a, even though the $\phi_{\text{GeSe-air}}^{\text{s (p)}}$ does not decrease with the increase of wavelength, its maintenance of a relatively low level makes the $\phi_{\text{GeSe-SiO}_2\text{-Si}}^{\text{s (p)}}$ become the domination in the denominator of Equation S23. More importantly, the $\phi_{\text{GeSe-SiO}_2\text{-Si}}^{\text{s (p)}}$ shares almost the same tendency with the refractive index of GeSe $n_{\text{AC(ZZ)}}$ in the concerned wavelength range. Therefore, it can be found in Figure S10b that changes in slope of the Equation S23 are rather slight with the increase of wavelength. As a result, the calculated relation between λ_{ope} and d_{GeSe} are almost linear in Figure S10c and identical to that demonstrated in Figure 5c of manuscript. In summary, $n_{\text{AC(ZZ)}}$ and

$\phi^{s\,(p)}_{\text{GeSe-SiO}_2\text{-Si}}$ sharing the similar decreasing tendency makes operating wavelength λ_{ope} (900~1300 nm) become almost linearly with the thickness of GeSe d_{GeSe} (125~200 nm). It is noted that the cases corresponding to the polarization anlge 0° and 90° are representative, and cases of other polarization anlge α can be calculated by replacing the $n_{\text{AC(ZZ)}}$ with $n(\alpha) = n_{\text{AC}}\cos\alpha + n_{\text{ZZ}}\sin\alpha$ to obtain $\phi_{\text{GeSe-air}}(\alpha)$ and $\phi_{\text{GeSe-SiO}_2\text{-Si}}(\alpha)$.

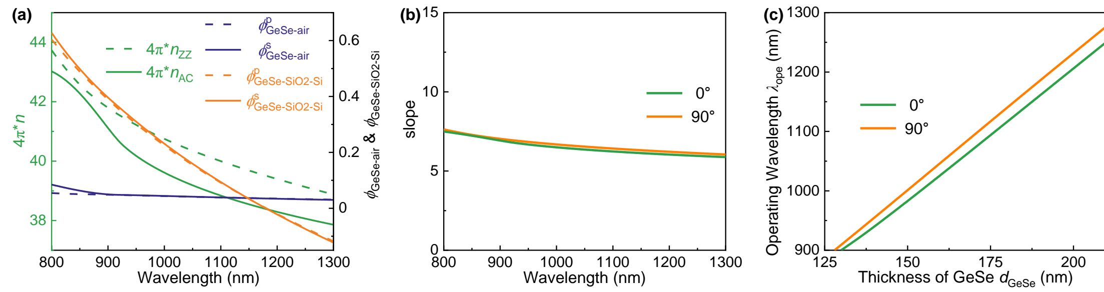

Figure S10 a) $4\pi{*}n_{\text{AC(ZZ)}}$ and $\phi^{s\,(p)}_{\text{GeSe-air}}$ as well as $\phi^{s\,(p)}_{\text{GeSe-SiO}_2\text{-Si}}$ (respectively the argument of the corrsponding amplitude reflection coefficient of s-(p-)light for air-GeSe structure and GeSe-SiO_2-Si structure) varied with the wavelength. b) Slope of Equation S23 for the polarization anlge 0° and 90°, corresponding to circumstances of s-light and p-light respectively. c) Calculated relation between operating wavelength λ_{ope} and thickness of GeSe d_{GeSe}.

S3.3 Experimentally Confirming Polarization-Sensitive Reconfigurable Perfect Absorber

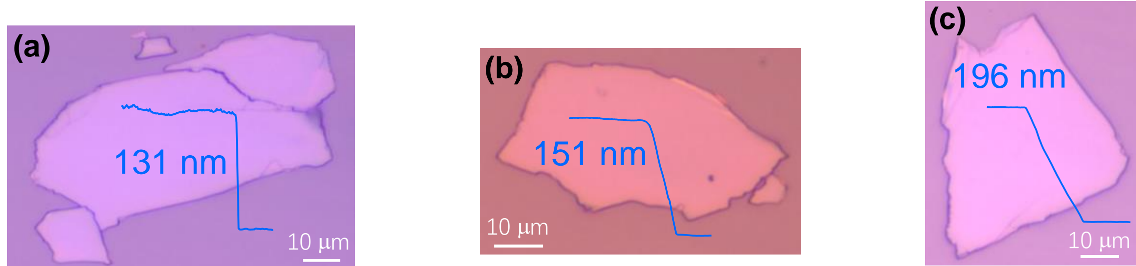

Figure S11. The exfoliated GeSe nanosheets with different thicknesses on Si substrate with a SiO_2 oxide layer (d_{SiO_2} = 200 nm), whose thickness are measured by atomic force microscope (AFM).

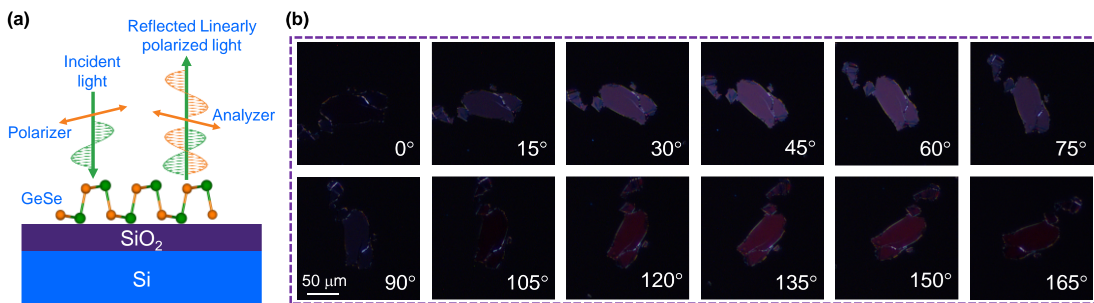

Figure S12. a) The schematic diagram of polarization-resolved optical microscopy (PROM). b) The PROM images under crossed-polarized light illumination with the 131-nm-thick GeSe nanosheet rotating from 0° to 180°.

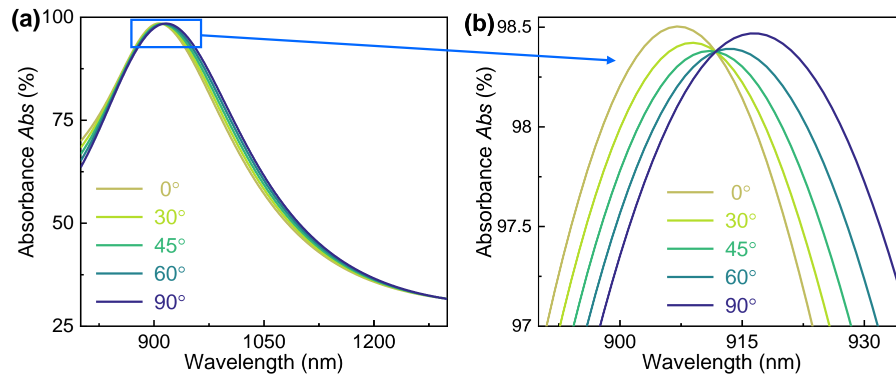

Figure S13. a) The theoretical result of *Abs* at the same d_{GeSe} (= 131 nm) and d_{SiO_2} (= 200 nm) of Figure 3e and 3f *versus* the α with b) its enlarged view at the peak.

Reference

[1] P. Petrik, M. Fried, T. Lohner, R. Berger, L. P. Bíró, C. Schneider, J. Gyulai, H. Ryssel, *Thin Solid Films* **1998**, 313-314, 259.

[2] B. Song, H. Gu, S. Zhu, H. Jiang, X. Chen, C. Zhang, S. Liu, *Appl. Surf. Sci.* **2018**, 439, 1079.

[3] a) H. Gu, B. Song, M. Fang, Y. Hong, X. Chen, H. Jiang, W. Ren, S. Liu, *Nanoscale* **2019**, 11, 22762; b) H. Fujiwara, *Spectroscopic ellipsometry: principles and applications*, John Wiley & Sons, Chichester, England **2007**.

[4] Z. Guo, H. Gu, M. Fang, B. Song, W. Wang, X. Chen, C. Zhang, H. Jiang, L. Wang, S. Liu, *ACS Mater. Lett.* **2021**, 3, 525.

[5] M. A. Kats, F. Capasso, *Laser & Photonics Rev.* **2016**, 10, 735.

[6] a) M. A. Kats, R. Blanchard, P. Genevet, F. Capasso, *Nat. Mater.* **2013**, 12, 20; b) Z. Li, S. Butun, K. Aydin, *ACS Photonics* **2015**, 2, 183.